NASA
Technical
Paper
3133

September 1991

P-52

Full-Scale Semispan Tests of a Business-Jet Wing With a Natural Laminar Flow Airfoil

David E. Hahne and
Frank L. Jordan, Jr.

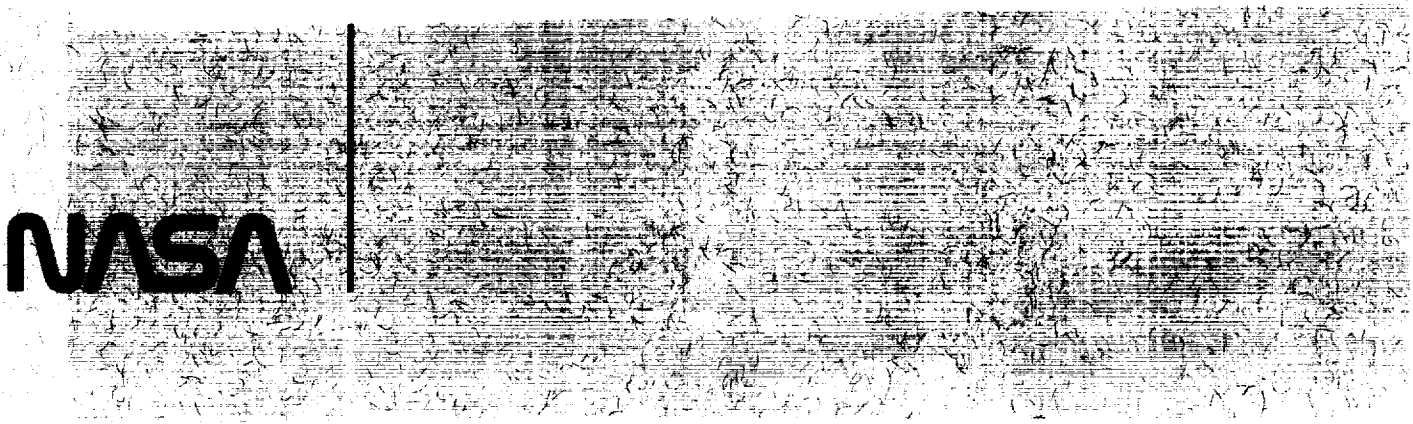

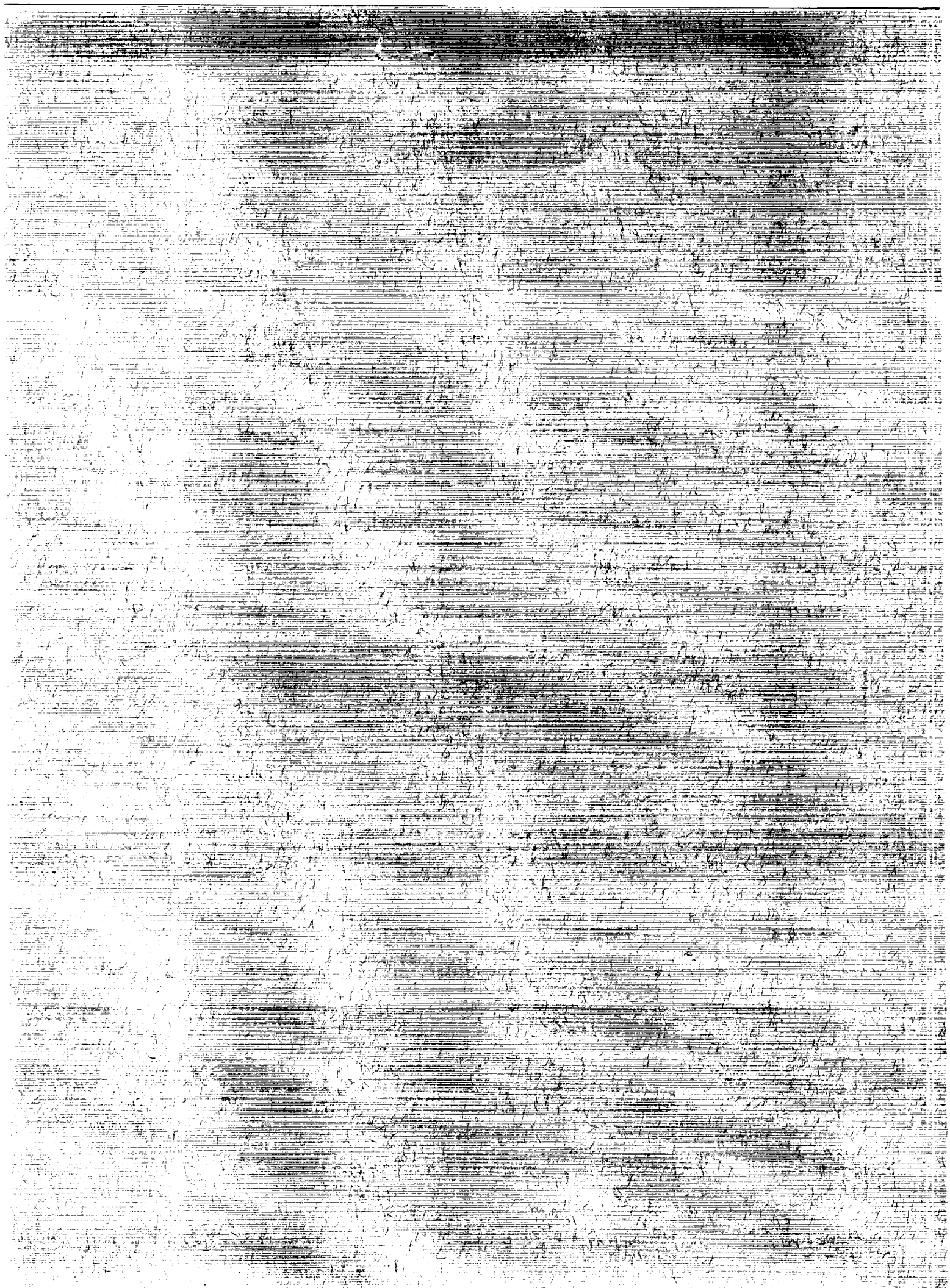

NASA Technical Paper 3133

1991

Full-Scale Semispan Tests of a Business-Jet Wing With a Natural Laminar Flow Airfoil

David E. Hahne and
Frank L. Jordan, Jr.
Langley Research Center
Hampton, Virginia

NASA
National Aeronautics and Space Administration
Office of Management
Scientific and Technical Information Program

The use of trademarks or names of manufacturers in this report is for accurate reporting and does not constitute an official endorsement, either expressed or implied, of such products or manufacturers by the National Aeronautics and Space Administration.

Abstract

An investigation was conducted in the Langley 30- by 60-Foot Tunnel on a full-scale semispan model to evaluate and document the low-speed, high-lift characteristics of a business-jet class wing that utilized the HSNLF(1)-0213 airfoil section and a single-slotted flap system. In addition to the high-lift studies, boundary-layer transition effects were examined, a segmented leading-edge droop for improved stall/spin resistance was studied, and two roll-control devices were evaluated.

The wind-tunnel investigation showed that deployment of a single-slotted, trailing-edge flap was effective in providing substantial increments in lift required for takeoff and landing performance. Fixed-transition studies to investigate premature tripping of the boundary layer indicated no adverse effects on lift and pitching-moment characteristics for either the cruise or landing configuration. The full-scale results also suggested the need to further optimize the leading-edge droop design that was developed in the subscale tests.

Introduction

While much research on natural laminar flow (NLF) airfoils has recently focused on drag reduction for improved cruise performance, few studies have addressed the use of high-lift systems for takeoff and landing with this wing class. Although large improvements in cruise performance have been shown, these NLF airfoils will only be used if they can be equipped with a viable flap system that is capable of generating enough lift to meet takeoff and landing requirements.

Prior to this investigation, some two-dimensional wind-tunnel tests had been conducted to evaluate high-lift characteristics of NLF airfoils and to support associated theoretical studies of flap effectiveness (refs. 1 and 2). These tests were focused on the use of simple split flaps. Other studies were conducted that used theoretical methods to design more complex flap systems for NLF airfoils (ref. 3). One of the airfoil sections used for the study in reference 3 was the high-speed HSNLF(1)-0213 airfoil. This airfoil was developed to extend the natural laminar flow concepts that were developed for low-speed airfoils to airfoils intended for higher speed and Reynolds number applications (refs. 4 to 6). As stated in references 6 and 7, the HSNLF(1)-0213 airfoil was designed for a cruise section lift coefficient of 0.26 at a Mach number of 0.7 and a Reynolds number of 9×10^6. Theoretical data on the airfoil predicted that large increments in lift could be obtained with a slotted flap design (ref. 3). As expected, the amount of additional lift and the angle of attack for maximum lift depended on the flap geometry. Two-dimensional theoretical studies indicated that a single-slotted flap design would offer a good trade-off between $C_{L,\max}$ and flap complexity for use on lightweight business jets (ref. 3). However, because theoretical techniques cannot reliably predict maximum lift for three-dimensional wings with flaps, experimental tests are necessary to accurately evaluate any flap system.

In the present investigation, tests were conducted in the Langley 30- by 60-Foot Tunnel on a full-scale semispan model that incorporated the HSNLF(1)-0213 airfoil section. The main objective of these tests was to evaluate and document the low-speed, high-lift characteristics of a business-jet class wing that used the HSNLF(1)-0213 airfoil section and a single-slotted flap system that was designed with the aid of the computer code described in reference 8. This flap system was the same as the one discussed in reference 4. Photographs of the model mounted for tests are shown in figure 1. Figure 1(a) shows the model with the flap retracted and the flow going from right to left. Figure 1(b) shows a close-up of the underside of the model with the flap deflected 40°. In addition to the high-lift studies, boundary-layer transition effects were examined, a segmented leading-edge droop for improved stall/spin resistance was studied, and two roll-control devices were evaluated.

Symbols

Longitudinal forces and moments are presented in the stability-axis system, and lateral forces and moments are presented in the body-axis system. A moment reference center of $0.25\bar{c}$ was used for all tests.

b	wing span, ft
C_D	drag coefficient, $\frac{\text{Drag}}{q_\infty S}$
C_L	lift coefficient, $\frac{\text{Lift}}{q_\infty S}$
$C_{L,\max}$	maximum lift coefficient
C_l	rolling-moment coefficient, $\frac{\text{Rolling moment}}{q_\infty S b/2}$
C_m	pitching-moment coefficient, $\frac{\text{Pitching moment}}{q_\infty S \bar{c}}$
C_p	pressure coefficient, $\frac{p - p_\infty}{q_\infty}$
ΔC_l	incremental rolling-moment coefficient
c	local wing chord with droop off, ft

$\bar{c}$	mean aerodynamic chord, ft
p	local static pressure, lb/ft^2
p_∞	free-stream static pressure, lb/ft^2
q_∞	free-stream dynamic pressure, lb/ft^2
R	Reynolds number based on $\bar{c}$
S	semispan reference area, ft^2
x	chordwise distance from wing leading edge, positive aft, ft
y	spanwise distance from wing root, ft
z	normal distance from wing leading edge, positive up, ft
α	angle of attack, deg
δ_a	aileron deflection, positive trailing edge down, deg
δ_f	flap deflection, positive trailing edge down, deg
δ_s	spoiler deflection, positive trailing edge up, deg

Abbreviations:

FS	fuselage station, in.
MCARF	Multi-Component Airfoil Analysis Program
NLF	natural laminar flow
VG	vortex generator
WS	wing station, measured plane of wing, in.

Model Description and Apparatus

The geometry of the semispan model tested is shown in figure 2, and a summary of the geometric characteristics is contained in table I. The HSNLF(1)-0213 airfoil section used in these tests is shown in figure 3, and section coordinates for this airfoil are given in table II. The wing incorporated 3° of twist between wing station 0.0 and the 50-percent semispan station. An additional 1° of twist was incorporated between the 50-percent semispan station and the wingtip for a total of 4° washout. The inboard portion of the wing was twisted about the 30-percent chord line, and the outboard portion of the wing was twisted about the 78-percent chord line. A small winglet was located at the wingtip. The model also incorporated an aileron and spoiler for roll control. (See fig. 2.) A half body of revolution was incorporated to simulate the presence of a fuselage near the wing. This fuselage was representative of a business jet in both size and shape. A vortex generator was mounted on the fuselage (fig. 4) just above the wing-body juncture to delay flow separation on the inboard panel of the wing. A multiposition flap system was incorporated in the model for evaluation. (See figs. 1(b) and 5.) The flap was a 28-percent chord flap that extended from the wing root to a semispan location of $2y/b = 0.79$. Flap deflections (0°, 20°, and 40°), flap gap, and flap overlap were set by changing three brackets that were located on the lower surface of the wing. Flap overlap was defined as the distance from the trailing edge of the wing upper surface ($0.92c$) to the leading edge of the flap (negative when the wing overlaps the flap). Flap gap was defined as the shortest vertical distance between the wing upper surface ($0.92c$) and the flap leading edge. The nominal flap overlap and gap were 0 and 2 percent of the local wing chord for the flap deflected 40° and −3 and 4 percent of the local wing chord for the flap deflected 20°.

In an attempt to improve stall/spin resistance, a segmented leading-edge droop was developed for the wing prior to the full-scale semispan tests. These exploratory tests used two subscale models. The models incorporated the same airfoil section and wing planform as the full-scale semispan model. However, the subscale model wings that were used for droop development were not twisted, and they did not incorporate a winglet. Static force tests, which were conducted in the Langley 12-Foot Low-Speed Tunnel at a Reynolds number of 3.1×10^5, were used to develop several candidate droop geometries. The roll-damping characteristics of these droop designs were then evaluated in dynamic force tests in the Langley 30- by 60-Foot Tunnel. This evaluation was used to select the final droop configuration for the full-scale tests. These roll-damping tests were conducted at a Reynolds number of 9.7×10^5. Reference 9 contains a description of the techniques used to develop this droop design. Figure 6 shows the leading-edge droop location and droop section that resulted from the subscale tests. The droop design consisted of two segments: an outboard segment that extended from the tip inboard to approximately the 70-percent semispan location and a smaller segment that was mounted farther inboard between the 40- and 50-percent semispan locations. The droop section was derived from another NLF airfoil (NLF(1)-0215F). This approach was adopted in an attempt to achieve natural laminar flow on the drooped as well as the undrooped portions of the wing. Coordinates for the drooped airfoil section are given in table III.

Unless otherwise noted, the data presented herein are for configurations that do not include the droop.

Static force and moment measurements were made in the Langley 30- by 60-Foot Tunnel with the external scale system that is described in reference 10. The loads on both the wing and the fuselage are included in all force and moment data. In addition to force and moment measurements, static-pressure data, flow visualization, and hot-film data were obtained. A total of 322 pressure taps were spaced along the span of the wing at eight stations: 20-, 35-, 45-, 55-, 62-, 75-, 85-, and 95-percent semispan locations. Chordwise locations of both the upper and lower surface ports are listed in table IV. A total of 45 hot-film sensors were mounted on the wing (both upper and lower surfaces) to measure boundary-layer behavior at three spanwise locations. (See fig. 7.) Surface tufts were used to visualize the surface flow conditions, especially stall progression. These tufts were removed while pressure and hot-film data were obtained.

Test Conditions and Corrections

Tests were conducted over an angle-of-attack range from $-10°$ to $40°$. Aerodynamic force and moment data were obtained at free-stream velocities of 55, 66, and 77 mph, which correspond to Reynolds numbers based on $\bar{c}$ of about 3.05×10^6, 3.67×10^6, and 4.26×10^6, respectively. Most of the tests were conducted at a free-stream velocity of 66 mph; unless otherwise noted, the data presented are for this condition. Although some roll data were taken to evaluate aileron and spoiler effectiveness, the tests focused on longitudinal characteristics of the semispan model.

A wind-tunnel calibration was made prior to model installation to determine buoyancy and flow angularity corrections. Flow-field surveys were made to determine flow blockage corrections in the manner described in reference 11. Corrections for jet boundary interference were made in accordance with the method of reference 12 and are described in references 13 to 15. The Langley 30- by 60-Foot Tunnel has a measured turbulence factor of 1.1, which corresponds to an average turbulence level of approximately 0.1 percent of the mean flow velocity (ref. 16).

Results and Discussion

Pressure Distributions

Chordwise pressure distributions for $\delta_f = 0°$ and $\delta_f = 40°$ are presented in figures 8 and 9. Data were obtained for angles of attack between $-2.2°$ and $16.8°$ at the eight semispan stations that were previously discussed. Problems with the pressure measurement system resulted in a limited amount of reliable pressure data. The pressure data presented in figure 8(b) for $\alpha = 1.5°$ with the flaps retracted ($C_L \approx 0.3$) show that pressure gradients are conducive to laminar flow over much of the upper and lower surfaces of the wing. This conduciveness is indicated by the decreasing values of the pressure coefficient with the chord station up to about the 60-percent chord station. These results indicate that, even at low speeds, the amount of laminar flow possible over the wing at cruise angles of attack should be significant.

A comparison of the pressure data in figures 8 and 9 ($\delta_f = 0°$ and $\delta_f = 40°$) indicates that large increases in lift result from flap deflection. Even though the vortex generator was on for the $\delta_f = 40°$ data, the generator was believed to have no effect on the pressure data because flow visualization studies indicated that the vortex generator primarily affected the flow inboard of the $2y/b = 0.2$ pressure port station. Integration of the pressure distribution data to calculate the lift on the wing and flap indicates that this increase in total lift results not only from the lift generated on the flap but also from the enhanced lift characteristics on the main wing.

Effect of Reynolds Number

The effect of Reynolds number on the longitudinal characteristics for the model without the vortex generator and with the flaps retracted is shown in figure 10. Changes in Reynolds number had no effect on lift characteristics except in the maximum lift and post-stall angle-of-attack regions. The increase in both the maximum lift coefficient and stall angle of attack at the higher Reynolds numbers resulted from the increased resistance of the boundary layer to separation. With the flaps deflected 40° and the vortex generator installed, Reynolds number effects on lift and pitching moment were limited to a small angle-of-attack range just past the stall. (See fig. 11.) The maximum lift coefficient and stall angle of attack, however, were not affected by Reynolds number variations.

Two-dimensional data from reference 7 for the basic airfoil with $\delta_f = 0°$ showed very little change in minimum drag for Reynolds numbers between 4.0×10^6 and 9.0×10^6 at low subsonic Mach numbers. However, these two-dimensional tests did indicate that there were some Reynolds number effects on maximum lift between $R = 4.0 \times 10^6$ and $R = 6.0 \times 10^6$. Since the full-scale data indicated virtually no Reynolds number effects between $R = 3.67 \times 10^6$ and $R = 4.26 \times 10^6$ (the maximum Reynolds number obtainable for these tests), the majority of these tests

were conducted at $R = 3.67 \times 10^6$ (66 mph). Unless noted otherwise, data presented herein are for this test condition.

Effect of Transition

With any NLF airfoil, there is always concern about the effect on the aerodynamic characteristics of premature boundary-layer transition that results from leading-edge contamination (e.g., dirt, insects, or scratches). In addition to performance impacts, the potential effect on aircraft stability characteristics must also be addressed. To evaluate the effect of early transition on the wing longitudinal characteristics, boundary-layer transition was fixed at a chord location of $x/c = 0.05$ on both the upper and lower surfaces of the wing by using the guidelines in reference 16. Tape with a serrated leading edge, ½ in. wide and 1/64 in. high, was used on the upper surface, and a double thickness of the same tape was used on the lower surface. Transition strips were not used on either the fuselage or wing flap. The effect of fixed transition on the aerodynamic coefficients can be seen in figure 12 for $\delta_f = 0°$. The data for this wing indicate a very slight loss in lift near $C_{L,\max}$, which probably resulted from early separation of the flow downstream of the boundary-layer trip. Pitch stability was also unaffected by tripping the boundary layer. This was expected because the airfoil was designed so that lift and pitching moment would be unaffected by premature transition. Figure 12(b) shows the effect of fixed transition on drag. There was an increase in C_D of 0.003 near $C_L = 0.3$ when the flow was tripped at $x/c = 0.05$. Data from two-dimensional tests (ref. 7) indicated a similar increase in C_D for similar test conditions (Reynolds number of 3.6×10^6 at $M < 0.3$). The effect of transition on the lift and pitching-moment characteristics for the flap deflected 40° is shown in figure 13. The addition of a transition strip did not significantly affect the longitudinal characteristics because very little, if any, laminar flow existed on the wing at such an extreme flap deflection. This result indicates that landing characteristics do not depend strongly on wing surface conditions.

Hot-film sensors were used to determine the extent of laminar flow on the wing with natural transition. A sample set of oscillograph tracings from the mid-semispan, hot-film sensors on the lower wing surface at a total C_L of 0.22 is shown in figure 14. The data were taken over a time period of 1.5 sec and show that the boundary-layer characteristics change rapidly over the chord. The tracing from the sensor at the 10-percent chord station shows that the boundary layer was laminar essentially 100 percent of the time. At points farther aft along the chord, the flow was mostly laminar with turbulent bursts. At 50 percent chord the boundary layer was turbulent 50 percent of the time. Aft of that location, the flow was predominantly turbulent with some laminar bursts. The transition point was the chord location where the boundary layer was turbulent 50 percent of the time. Therefore, for this example, laminar flow existed back to 50 percent chord.

Figure 15 shows the extent of laminar flow on the upper and lower surfaces at three spanwise locations as a function of total lift coefficient. Figure 15(a) shows that there was significant laminar flow on the upper surface for lift coefficients that range from −0.40 to about 0.22. A reduction in laminar flow was seen with increasing C_L above 0.22. (The next data point was at $C_L = 0.31$, so the initial reduction in laminar flow could conceivably occur at a lift coefficient that is slightly higher than 0.22.) Figure 15(b) shows that there was essentially no laminar flow on the lower surface for lift coefficients below 0.22 but that there was significant laminar flow on the lower surface for lift coefficients greater than 0.22. Combining the results for the upper and lower surfaces indicates that the optimum C_L for maximizing the extent of laminar flow over the wing is about 0.22 or slightly higher.

Because of three-dimensional effects (e.g., the variation of local Reynolds number along the span), the extent of laminar flow was not constant along the span. The maximum amount of laminar flow on the upper surface was 60 percent of the chord (outboard station), and the minimum amount was 35 percent of the chord (inboard station). The average amount of laminar flow on the upper surface was less than 50 percent. The lower surface characteristics were similar, with a laminar flow maximum of 70 percent (outboard station), a minimum of 30 percent (inboard station), and an average of about 50 percent. The correlation of the hot-film results with the favorable pressure gradient characteristics discussed previously was good. This correlation indicates that the extent of laminar flow was not being significantly affected by small surface irregularities. The amount of laminar flow in the two-dimensional tests (ref. 5) was 40 to 50 percent on the upper surface and 50 to 60 percent on the lower surface.

Effect of Flap Deflection

The single-slotted flap used in these tests was designed with the MCARF (Multi-Component Airfoil Analysis Program) computer code (ref. 8), which was developed to analyze two-dimensional airfoil-flap configurations. Because this code cannot accurately

model trailing-edge separation, it relies on the assumption of laminar separation near the leading edge to predict stall. Thus, the code tends to overpredict $C_{L,\max}$ when the trailing edge stalls first. Test results from an evaluation of flap overlap and gap settings with the flap deflected 40° indicated that the optimum flap location predicted by the theoretical code did achieve the best $C_{L,\max}$ experimentally (0-percent overlap and 2-percent gap). All data presented with the flaps deflected 40° were obtained with the optimum gap and overlap values. The overlap and gap for the 20° flap deflection, which were based on the MCARF predictions, were fixed at −3 and 4 percent.

Longitudinal characteristics for the semispan model for flap deflections of 0°, 20°, and 40° with the vortex generator mounted are presented in figure 16. With 0° flap deflection, a $C_{L,\max}$ of 1.45 was achieved at an angle of attack of about 17° (fig. 16(a)). The pitching-moment data showed no unstable breaks in the curves and generally showed linear behavior up to $C_{L,\max}$. The C_L data showed that sizable increments in lift were achieved by deflecting the trailing-edge flap ($C_{L,\max} = 2.44$). This result is representative of other single-slotted flap designs. As expected, the value of $C_{L,\max}$ that was predicted by the code was higher than the measured value; however, the increment in lift due to flap deflection was accurately predicted.

The increase in lift seen in figure 16(a) resulted in a corresponding increase in nose-down pitching moment that was fairly linear with flap deflection at low and moderate angles of attack. Flap deflection had little effect on the overall level of pitch stability below 15° angle of attack. The pitching-moment break at the stall with the flaps deflected 40°, however, was slightly unstable in contrast to the flaps-undeflected configuration, which showed a slight stable break at stall. As expected, increasing the flap deflection increased the drag for a given value of C_L. (See fig. 16(b).) Unlike the lift and pitching-moment data, the changes in drag were nonlinear with flap deflection.

Effect of Vortex Generator

To alleviate premature flow separation on the inboard section of the wing, a fuselage-mounted vortex generator was investigated. (See fig. 4.) This premature flow separation was most clearly seen in tuft studies with the flaps deflected 40°. (See fig. 17.) Without the vortex generator, a large portion of the inboard panel was stalled. The addition of the vortex generator greatly reduced the region of stalled flow and delayed the progression of separated flow from the inboard to the outboard panel to higher angles of attack.

Figure 18 shows the effect of the vortex generator on the longitudinal characteristics of the semispan model with the flap undeflected. As can be seen from the data, the addition of the vortex generator improved $C_{L,\max}$ and delayed the stall by 2° angle of attack. Pitching moment and drag (figs. 18(a) and 18(b)) were unaffected by the vortex generator, except for negligible changes in the stall and post-stall angle-of-attack regions. The effect of the vortex generator with the flaps deflected 40° was more pronounced. (See fig. 19.) With the flaps deflected, maintaining attached flow over the inboard portion of the wing through the use of the vortex generator had a large beneficial effect, which increased $C_{L,\max}$ from 2.3 to 2.45. As with the flaps undeflected, pitching moment was essentially unaffected by the vortex generator.

Effect of Leading-Edge Droop

The concept of incorporating a discontinuous leading-edge droop on the outboard portion of a wing to improve stall/spin resistance characteristics has received much attention in recent years (refs. 9, 17, and 18). The purpose of the droop is to maintain attached flow on the outer wing panel to higher angles of attack to soften the stall break and to improve roll damping and roll control in the stall and post-stall regions. These improvements help to both prevent and control any autorotative tendencies of the aircraft. In most previous applications, a single outboard droop segment has been sufficient to prevent autorotative tendencies. (See ref. 17.) However, recent studies have shown that wings with relatively high aspect ratios require an additional segment located farther inboard to achieve the desired stall/spin resistance characteristics. As mentioned previously, the leading-edge droop for the subject configuration was developed on two subscale models, and the droop configurations were evaluated with both static force data and roll-damping data. Results from these tests (ref. 17) showed that the selected droop should provide the desired stall/spin resistance characteristics.

Figure 20 shows the effect of the droop on the flap-retracted configuration that was measured during the full-scale semispan model tests. The addition of the droop did not significantly improve the lift characteristics until well into the post-stall region. The fact that the desired "flat top" lift curve was not obtained suggests that the droop design may not provide the improved stall characteristics shown in the subscale tests. However, the effectiveness of a leading-edge droop is not always apparent from an examination

of total lift characteristics. In most cases, the effect of the droop on static characteristics can best be seen by separately measuring the forces on the outer panel of the wing. This approach was used during the original droop design but was impractical for the semispan tests. Because the droop was developed on a wing without twist, without a winglet, and at very low Reynolds numbers, the design might not have been properly optimized for the full-scale semispan model. The effect of the droop on drag was negligible around the design cruise lift coefficient of 0.26. Thus, the goal of maintaining natural laminar flow on the drooped portion of the wing was achieved.

Roll-Control Effectiveness

Roll-control data in the form of rolling-moment increments are shown in figures 21 to 23. Data for the wing without the droop and with the flap undeflected (fig. 21) show that the aileron was effective in providing roll control well past $C_{L,\max}$. Additional roll control was obtained by deflecting the spoiler. Once the wing stalls in the spoiler region, the spoiler becomes ineffective. With the flaps deflected, the additional rolling moment from the spoiler was even more pronounced (fig. 22). Because the spoiler was in front of the flap (fig. 2) the larger lift increment generated by the flap was lost when the spoiler was deflected, thus creating these large rolling moments. Since the aileron was outboard of the flap, the effectiveness of the aileron was only slightly affected by the deflection of the flap (fig. 22). The effect of the leading-edge droop on the rolling moment is shown in figure 23 for $\delta_f = 0°$ and $\delta_a = 20°$. The data show a sizable improvement in roll control above $\alpha = 5°$ with the addition of the droop. This result indicates that the droop was affecting the flow on the outboard portion of the wing, even though the total lift data showed no effect from the droop. This result indicates a delay in separation of the flow on the outboard panel and illustrates that changes in roll control can be used to some degree to evaluate droop effectiveness when a metric outboard panel is impractical to use.

Summary of Results

A wind-tunnel investigation of the high-lift characteristics of a full-scale semispan wing with a natural laminar flow airfoil was conducted in the Langley 30- by 60-Foot Tunnel. The results of these tests can be summarized as follows:

1. Deployment of a single-slotted, trailing-edge flap provided substantial increments in lift without significant adverse effects on static pitch stability. These results suggest that an NLF wing designed for efficient cruise at Mach 0.7 can also be viable at low-speed takeoff and landing conditions.
2. Fixed-transition studies indicated no adverse effects on lift and pitching-moment characteristics as a result of the transition of the boundary layer near the leading edge for either the cruise or landing configuration.
3. Maximum lift coefficient was improved by using a fuselage-mounted vortex generator to delay separation of the flow on the inboard portion of the wing.
4. Although roll-control studies indicated some delay in outboard-panel flow separation, the full-scale data suggest the need for further optimization of the leading-edge droop design to provide improved stall/spin resistance.
5. The wing aileron provided good roll control up to stall. Additional rolling moment was generated by a midspan spoiler for flap deflections of 0° and 40°. The effectiveness of the spoiler was significantly greater with the trailing-edge flap deflected.

NASA Langley Research Center
Hampton, VA 23665-5225
August 6, 1991

References

1. Somers, Dan M.: *Design and Experimental Results for a Natural-Laminar-Flow Airfoil for General Aviation Applications.* NASA TP-1861, 1981.
2. McGhee, Robert J.; Viken, Jeffrey K.; Pfenninger, Werner; Beasley, William D.; and Harvey, William D.: *Experimental Results for a Flapped Natural-Laminar-Flow Airfoil With High Lift/Drag Ratio.* NASA TM-85788, 1984.
3. Morgan, Harry L.: High-Lift Flaps for Natural Laminar Flow Airfoils. *Laminar Flow Aircraft Certification,* Louis J. Williams, compiler, NASA CP-2413, 1986, pp. 31–65.
4. Harvey, William D.: Boundary-Layer Control for Drag Reduction. *International Pacific Air & Space Technology Conference Proceedings,* P-208, Soc. of Automotive Engineers, Inc., 1988, pp. 287–311. (Available as SAE Paper 872434.)
5. Harvey, W. D.; McGhee, R. J.; and Harris, C. D.: Wind Tunnel Testing of Low-Drag Airfoils. *Laminar Flow Aircraft Certification,* Louis J. Williams, compiler, NASA CP-2413, 1986, pp. 89–128.
6. Sewall, William G.; McGhee, Robert J.; Viken, Jeffrey K.; Waggoner, Edgar G.; Walker, Betty S.; and Millard,

Betty F.: *Wind Tunnel Results for a High-Speed, Natural Laminar-Flow Airfoil Designed for General Aviation Aircraft.* NASA TM-87602, 1985.

7. Sewall, William G.; McGhee, Robert J.; Hahne, David E.; and Jordan, Frank L., Jr.: *Wind Tunnel Results of the High-Speed NLF(1)-0213 Airfoil. Research in Natural Laminar Flow and Laminar-Flow Control,* Jerry N. Hefner and Frances E. Sabo, compilers, NASA CP-2487, Part 3, 1987, pp. 697 726.

8. Stevens, W. A.; Goradia, S. H.; and Braden, J. A.: *Mathematical Model for Two-Dimensional Multi-Component Airfoils in Viscous Flow.* NASA CR-1843, 1971.

9. Staff of Langley Research Center: *Exploratory Study of the Effects of Wing-Leading-Edge Modifications on the Stall/Spin Behavior of a Light General Aviation Airplane.* NASA TP-1589, 1979.

10. DeFrance, Smith J.: *The N.A.C.A. Full-Scale Wind Tunnel.* NACA Rep. 459, 1933.

11. Theodorsen, Theodore; and Silverstein, Abe: *Experimental Verification of the Theory of Wind-Tunnel Boundary Interference.* NACA Rep. 478, 1934.

12. Heyson, Harry H.: *Use of Superposition in Digital Computers To Obtain Wind-Tunnel Interference Factors for Arbitrary Configurations, With Particular Reference to V/STOL Models.* NASA TR R-302, 1969.

13. Heyson, Harry H.: *FORTRAN Programs for Calculating Wind-Tunnel Boundary Interference.* NASA TM X-1740, 1969.

14. Heyson, Harry H.: *Nomographic Solution of the Momentum Equation for VTOL-STOL Aircraft.* NASA TN D-814, 1961.

15. Heyson, Harry H.: *Rapid Estimation of Wind-Tunnel Corrections With Application to Wind-Tunnel and Model Design.* NASA TN D-6416, 1971.

16. Rae, William H., Jr.; and Pope, Alan: *Low-Speed Wind Tunnel Testing,* Second ed. John Wiley & Sons, Inc., c.1984.

17. Johnson, Joseph L., Jr.; Yip, Long P.; and Jordan, Frank L., Jr.: Preliminary Aerodynamic Design Considerations for Advanced Laminar Flow Aircraft Configurations. *Laminar Flow Aircraft Certification,* Louis J. Williams, compiler, NASA CP-2413, 1986, pp. 185 225.

18. Stough, H. Paul, III; Jordan, Frank L., Jr.; DiCarlo, Daniel J.; and Glover, Kenneth E.: Leading-Edge Design for Improved Spin Resistance of Wings Incorporating Conventional and Advanced Airfoils. *Langley Symposium on Aerodynamics,* Volume II, Sharon H. Stack, compiler, NASA CP-2398, 1985, pp. 141- 157.

Table I. Geometric Characteristics of Semispan Model

Wing:	
Semispan area, ft^2	125.00
Semispan, ft	22.36
Mean aerodynamic chord, ft	6.15
Root chord (centerline), ft	8.28
Tip chord, ft	2.91
Aspect ratio of semispan	4.00
Wing incidence (root), deg	2.00
Dihedral angle of leading edge, deg	5.50
Leading-edge sweep angle, deg	4.15
Fuselage station of wing leading edge (centerline), in.	225.18
Airfoil	NASA HSNLF(1)-0213
Flap:	
Area, ft^2	24.30
Inboard wing station, in.	32.20
Outboard wing station, in.	211.99
Chord, percent c	28.00
Aileron:	
Area, ft^2	4.39
Inboard wing station, in.	211.99
Outboard wing station, in.	264.86
Chord, percent c	28.00
Hinge line, percent c	78.00
Spoiler:	
Area, ft^2	3.20
Inboard wing station, in.	114.05
Outboard wing station, in.	173.62
Chord, percent c	12.00
Hinge line, percent c	78.00
Trailing edge, percent c	92.00
Fuselage:	
Length, ft	35.00
Radius (maximum), ft	2.50
Winglet:	
Area, ft^2	0.65
Span, ft	0.88
Root chord, ft	1.06
Tip chord, ft	0.43
Aspect ratio	1.19
Cant angle (outboard), deg	20.50
Leading-edge sweep angle, deg	45.00
Airfoil	NACA 0012-35

Table II. HSNLF(1)-0213 Airfoil Coordinates

x/c	Upper surface z/c	Lower surface z/c
0.00000	0.00000	0.00000
0.00123	0.00676	−0.00257
0.00270	0.01001	−0.00450
0.00499	0.01350	−0.00713
0.00801	0.01688	−0.00983
0.01177	0.01995	−0.01191
0.01627	0.02309	−0.01399
0.02147	0.02602	−0.01603
0.03389	0.03167	−0.01993
0.04104	0.03438	−0.02181
0.04881	0.03705	−0.02364
0.06619	0.04222	−0.02724
0.07577	0.04470	−0.02902
0.08992	0.04711	−0.03078
0.09661	0.04945	−0.03254
0.10783	0.05170	−0.03427
0.11955	0.05387	−0.03597
0.13176	0.05596	−0.03765
0.14444	0.05796	−0.03928
0.15759	0.05985	−0.04088
0.17119	0.06166	−0.04242
0.19963	0.06494	−0.04532
0.21445	0.06641	−0.04670
0.24519	0.06901	−0.04933
0.27723	0.07110	−0.05174
0.29370	0.07195	−0.05286
0.31042	0.07266	−0.05392
0.34457	0.07365	−0.05583
0.36193	0.07392	−0.05667
0.37942	0.07405	−0.05741
0.39705	0.07402	−0.05807
0.41481	0.07384	−0.05864
0.43267	0.07350	−0.05911
0.45056	0.07299	−0.05948
0.48633	0.07147	−0.05990
0.50416	0.07043	−0.06000
0.52193	0.06920	−0.06003
0.55725	0.06605	−0.05969
0.57474	0.06411	−0.05933
0.60918	0.05940	−0.05821
0.62604	0.05664	−0.05743
0.64263	0.05362	−0.05645
0.67493	0.04699	−0.05385
0.70586	0.03996	−0.05002
0.73539	0.03300	−0.04450
0.75006	0.02953	−0.04115

Table II. Concluded

x/c	Upper surface z/c	Lower surface z/c
0.77995	0.02256	−0.03565
0.79503	0.01914	−0.03365
0.84008	0.00941	−0.02890
0.86896	0.00372	−0.02630
0.88077	0.00154	−0.02535
0.90712	−0.00298	−0.02315
0.94150	−0.00812	−0.02040
0.96027	−0.01057	−0.01895
0.97556	−0.01244	−1.01800
0.98718	−0.01380	−0.01750
1.00000	−0.01528	−0.01660

Table III. Drooped Airfoil Coordinates

x/c	Upper surface z/c	Lower surface z/c
−0.02000	−0.00988	−0.00988
−0.01975	−0.00792	−0.01157
−0.01950	−0.00636	−0.01285
−0.01900	−0.00575	−0.01332
−0.01850	−0.00467	−0.01410
−0.01800	−0.00369	−0.01475
−0.01750	−0.00279	−0.01531
−0.01500	0.00106	−0.01741
−0.01000	0.00686	−0.02007
0.00000	0.01468	−0.02329
0.01000	0.02075	−0.02540
0.02000	0.02584	−0.02697
0.03000	0.03024	−0.02824
0.04000	0.03407	−0.02934
0.05000	0.03749	−0.03033
0.06000	0.04054	−0.03126
0.08000	0.04576	−0.03307
0.09000	0.04804	−0.03399
0.10000	0.05013	−0.03494
0.12500	0.05480	−0.03745
0.15000	0.05876	−0.04014
0.15759	0.05985	−0.04088
0.17119	0.06166	−0.04242
0.19963	0.06494	−0.04532
0.21445	0.06641	−0.04670
0.24519	0.06901	−0.04933
0.27723	0.07110	−0.05174
0.29370	0.07195	−0.05286
0.31042	0.07266	−0.05392
0.34457	0.07365	−0.05583
0.36193	0.07392	−0.05667
0.37942	0.07405	−0.05741
0.39705	0.07402	−0.05807
0.41481	0.07384	−0.05864
0.43267	0.07350	−0.05911
0.45056	0.07299	−0.05948
0.48633	0.07147	−0.05990
0.50416	0.07043	−0.06000
0.52193	0.06920	−0.06003
0.55725	0.06605	−0.05969
0.57474	0.06411	−0.05933
0.60918	0.05940	−0.05821
0.62604	0.05664	−0.05743
0.64263	0.05362	−0.05645
0.67493	0.04699	−0.05385
0.70586	0.03996	−0.05002

Table III. Concluded

x/c	Upper surface z/c	Lower surface z/c
0.73539	0.03300	−0.04450
0.75006	0.02953	−0.04115
0.77995	0.02256	−0.03565
0.79503	0.01914	−0.03365
0.84008	0.00941	−0.02890
0.86896	0.00372	−0.02630
0.88077	0.00154	−0.02535
0.90712	−0.00298	−0.02315
0.94150	−0.00812	−0.02040
0.96027	−0.01057	−0.01895
0.97556	−0.01244	−0.01800
0.98718	−0.01380	−0.01750
1.00000	−0.01528	−0.01660

Table IV. Chordwise Location of Pressure Ports

[Wing, aileron, and spoiler port locations given in percent of local wing chord; flap port locations given in percent of local flap chord]

Station 1	Station 2	Station 3	Station 4	Station 5	Station 6	Station 7	Station 8
Wing upper surface							
2.5	2.5	2.5	2.5	2.5	2.5	2.5	2.5
5.0	5.0	5.0	5.0	5.0	5.0	5.0	5.0
7.5	7.5	7.5	7.5	7.5	7.5	7.5	7.5
10.0	10.0	10.0	10.0	10.0	10.0	10.0	10.0
15.0	15.0	15.0	15.0	15.0	15.0	15.0	15.0
20.0	20.0	20.0	20.0	20.0	20.0	20.0	20.0
25.0	25.0	25.0	25.0	25.0	25.0	25.0	25.0
30.0	30.0	30.0	30.0	30.0	30.0	30.0	30.0
40.0	40.0	40.0	40.0	40.0	40.0	40.0	40.0
50.0	50.0	50.0	50.0	50.0	50.0	50.0	50.0
60.0	60.0	60.0	60.0	60.0	60.0	60.0	60.0
70.0	70.0	70.0	70.0	70.0	70.0	70.0	70.0
80.0	80.0	79.0	79.0	79.0	80.0		
90.0	90.0				90.0		
Wing lower surface							
2.5	2.5	2.5	2.5	2.5	2.5	2.5	2.5
5.0	5.0	5.0	5.0	5.0	5.0	5.0	5.0
7.5	7.5	7.5	7.5	7.5	7.5	7.5	7.5
10.0	10.0	10.0	10.0	10.0	10.0	10.0	10.0
15.0	15.0	15.0	15.0	15.0	15.0	15.0	15.0
20.0	20.0	20.0	20.0	20.0	20.0	20.0	20.0
25.0	25.0	25.0	25.0	25.0	25.0	25.0	25.0
30.0	30.0	30.0	30.0	30.0	30.0	30.0	30.0
40.0	40.0	40.0	40.0	40.0	40.0	40.0	40.0
50.0	50.0	50.0	50.0	50.0	50.0	50.0	50.0
60.0	60.0	60.0	60.0	60.0	60.0	60.0	60.0
70.0	70.0	70.0	70.0	70.0	70.0	70.0	70.0
Flap upper surface							
2.49	2.50	2.50	2.51	2.51	2.52		
4.98	5.00	5.00	4.99	5.02	5.03		
9.96	10.00	10.00	10.02	10.03	10.06		
19.91	20.00	20.00	20.04	20.06	20.11		
28.88	28.89	29.01	29.07	29.09	29.16		
49.78	49.98	50.02	50.11	50.16	50.28		
72.88	73.16	73.22	73.36	73.43	73.61		
90.70	91.06	91.13	91.29	91.39	91.61		

Table IV. Concluded

Station 1	Station 2	Station 3	Station 4	Station 5	Station 6	Station 7	Station 8
Flap lower surface							
2.49	2.50	2.50	2.51	2.51	2.52		
4.98	5.00	5.00	4.99	5.02	5.03		
9.96	10.00	10.00	10.02	10.03	10.06		
19.91	20.00	20.00	20.04	20.06	20.11		
28.88	28.89	29.01	29.07	29.09	29.16		
49.78	49.98	50.02	50.11	50.16	50.28		
64.02	64.27	64.16	64.44	64.50	64.66		
72.88	73.16	73.22	73.36	73.43	73.61		
90.70	91.06	91.13	91.29	91.39	91.61		
Aileron upper surface							
						82.91	76.60
						91.45	88.30
						93.59	91.23
						97.86	97.08
Aileron lower surface							
						82.91	76.60
						91.45	88.30
						93.59	91.23
						97.86	97.08
Spoiler surface							
		90.01	92.84	90.03			

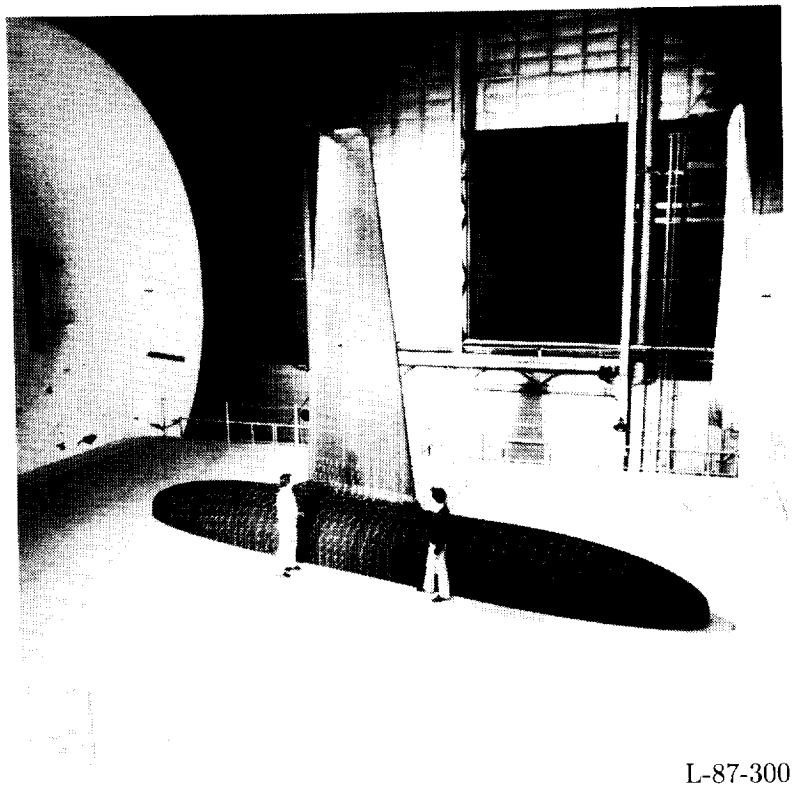

L-87-300

(a) Cruise configuration.

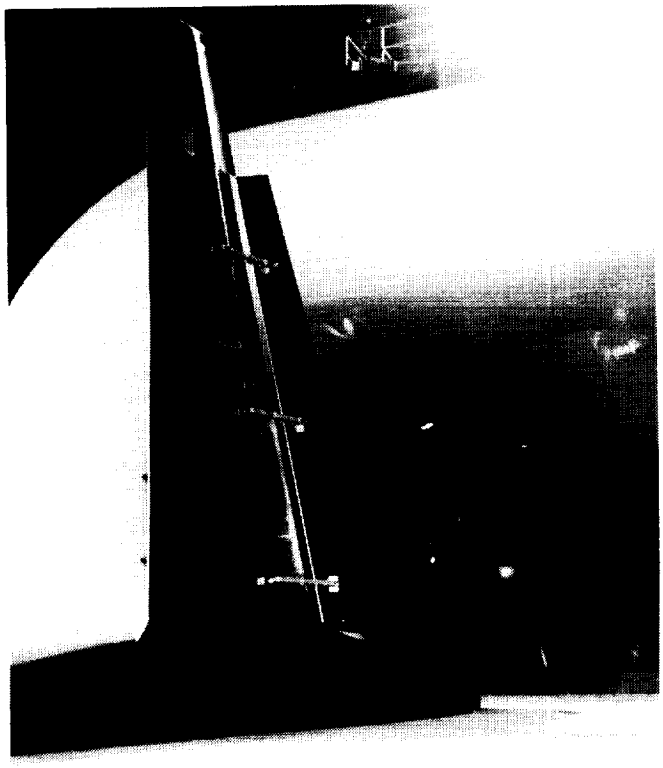

L-87-1234

(b) Flap deflected 40°.

Figure 1. Photographs of model in Langley 30- by 60-Foot Tunnel.

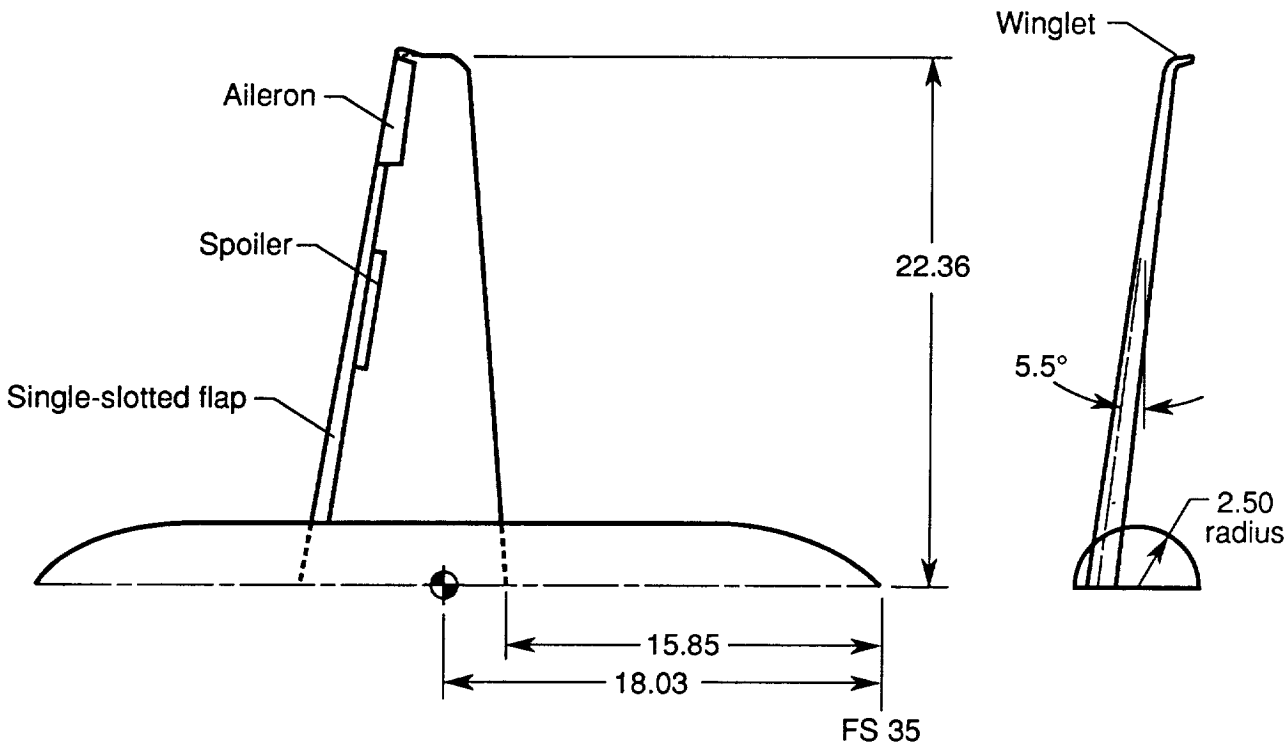

Figure 2. Geometry of semispan model. All dimensions in feet unless otherwise noted.

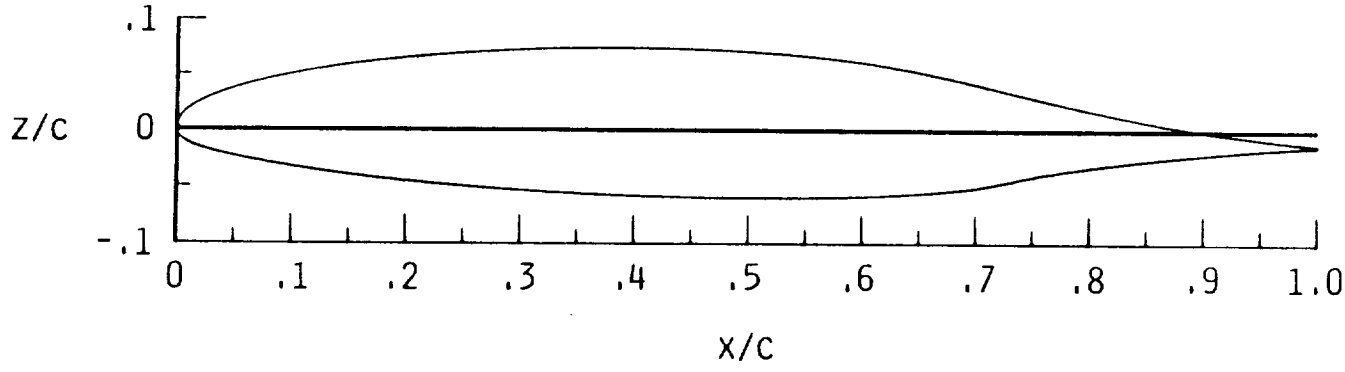

Figure 3. Section shape for HSNLF(1)-0213 airfoil.

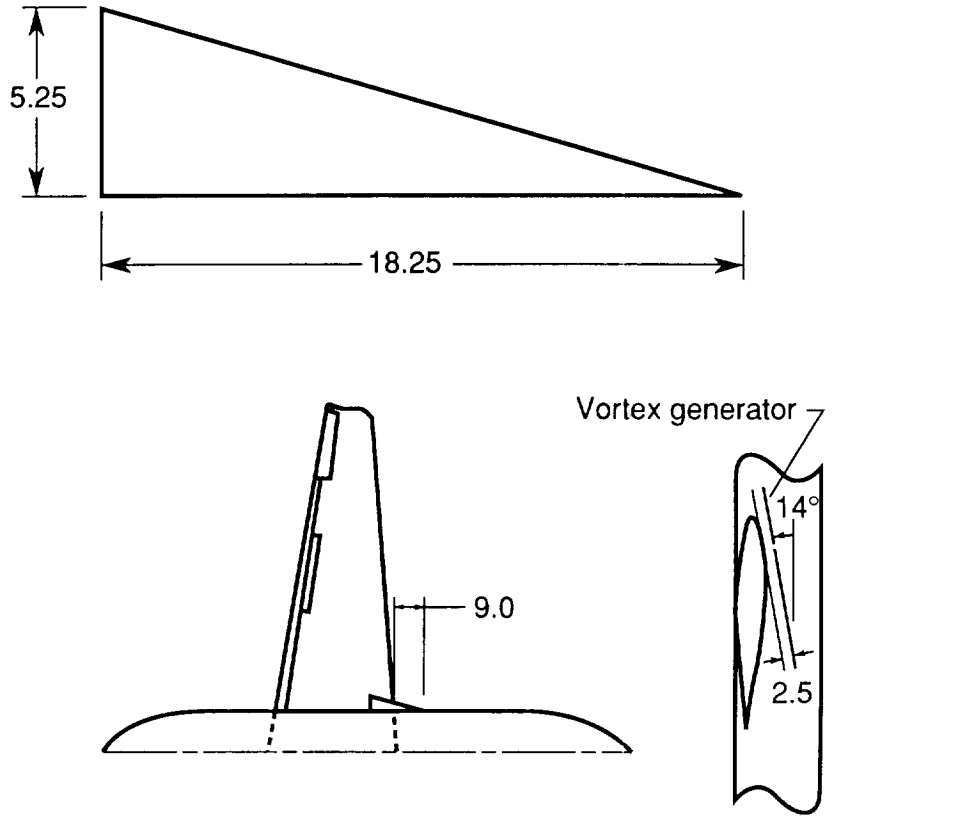

Figure 4. Geometry of vortex generator. All dimensions in inches unless otherwise noted.

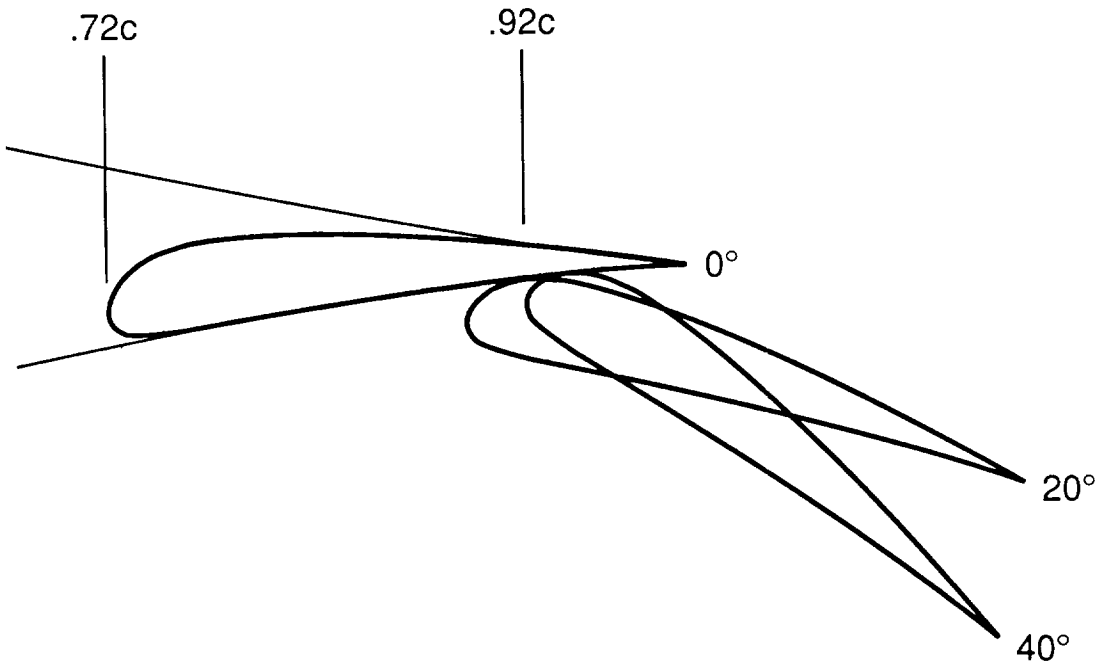

Figure 5. Geometry of trailing-edge flap.

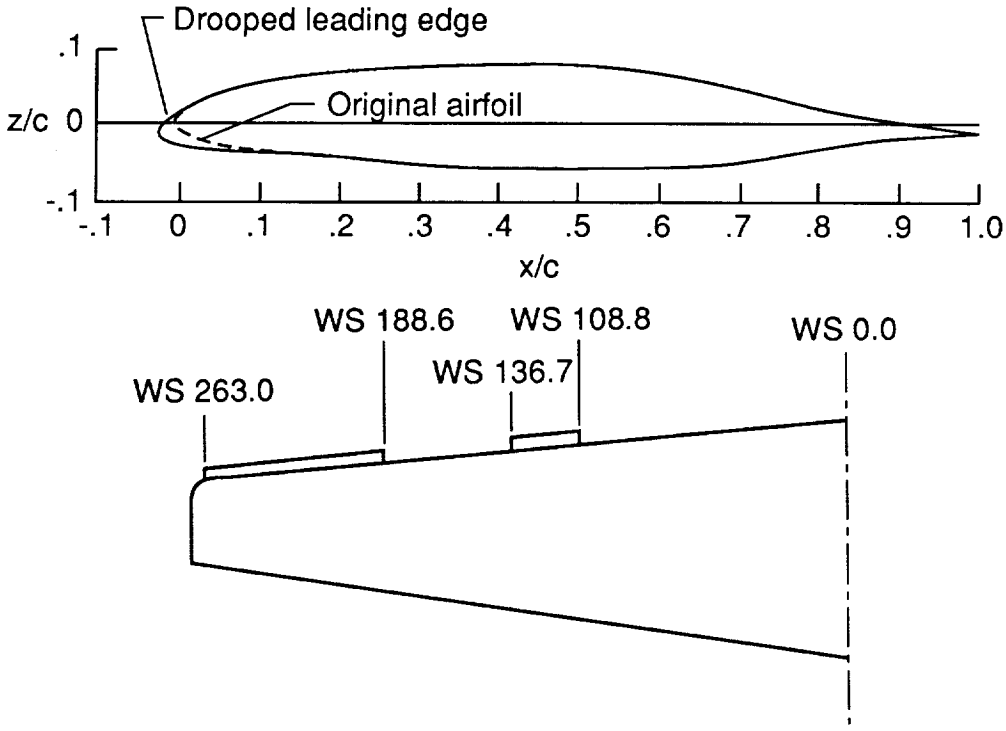

Figure 6. Geometry of leading-edge droop. Planform view not to scale.

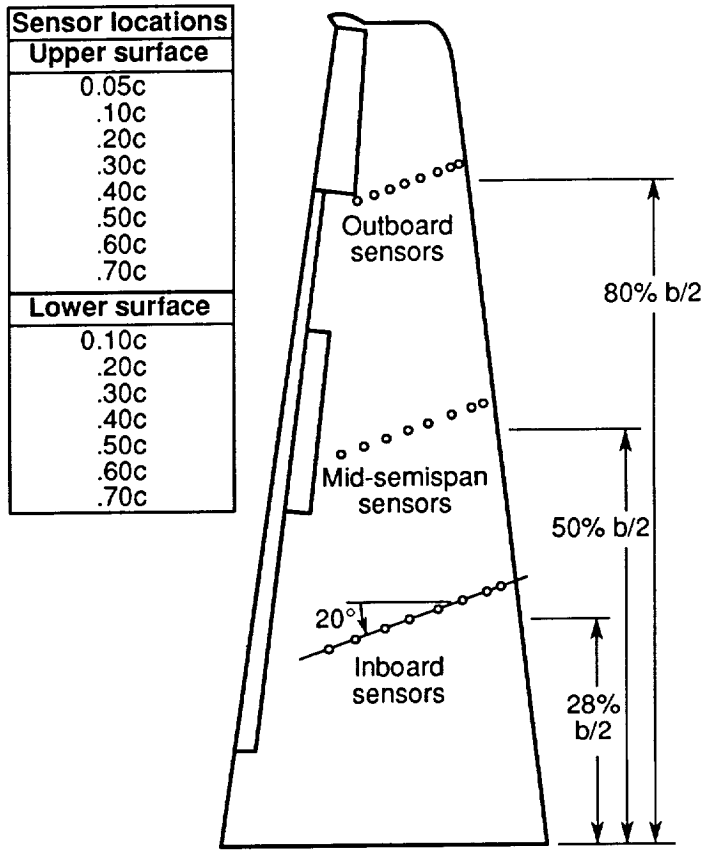

Figure 7. Locations of hot-film sensors.

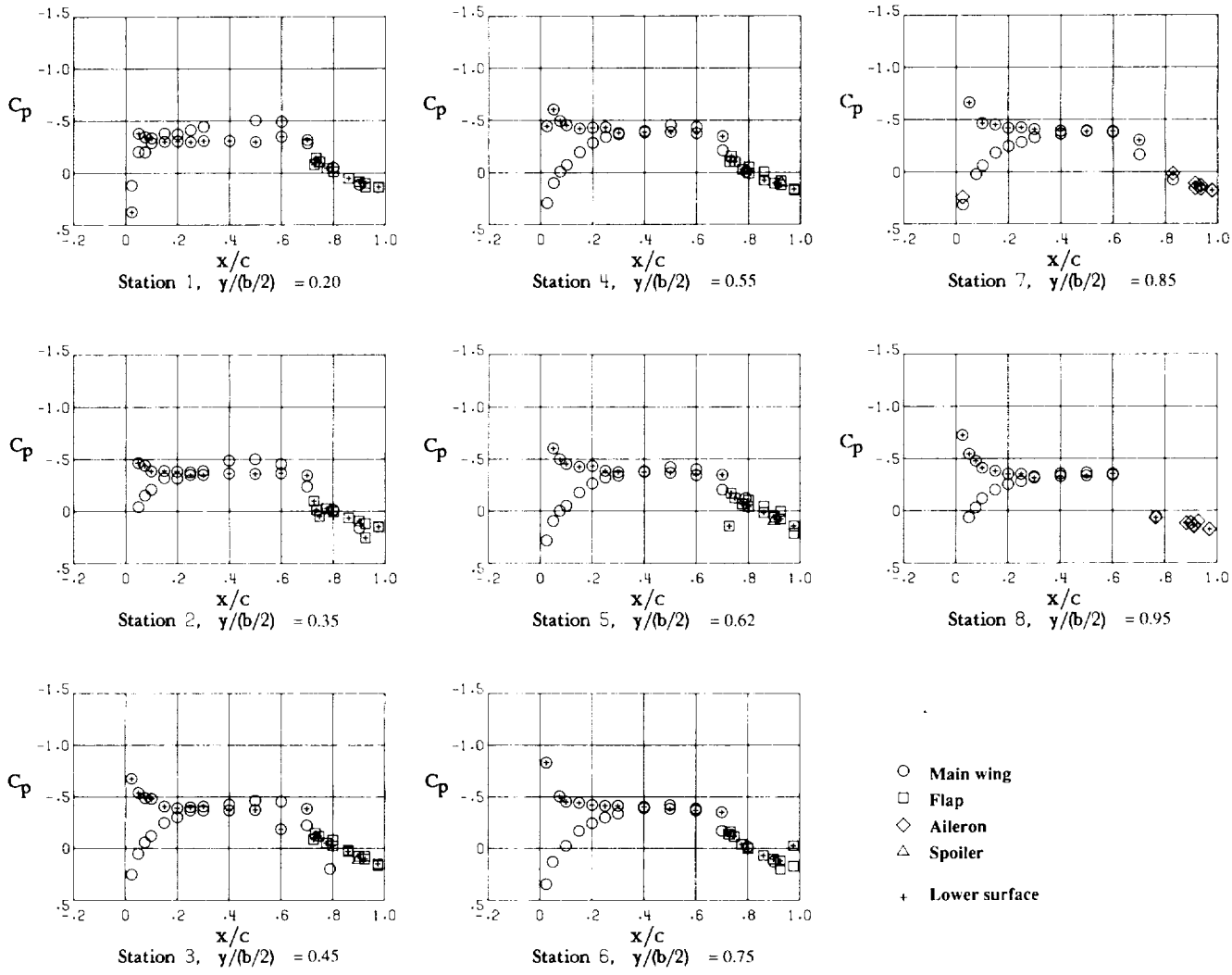

(a) $\alpha = -2.2°$.

Figure 8. Pressure distributions for clean wing. $\delta_f = 0°$; VG off.

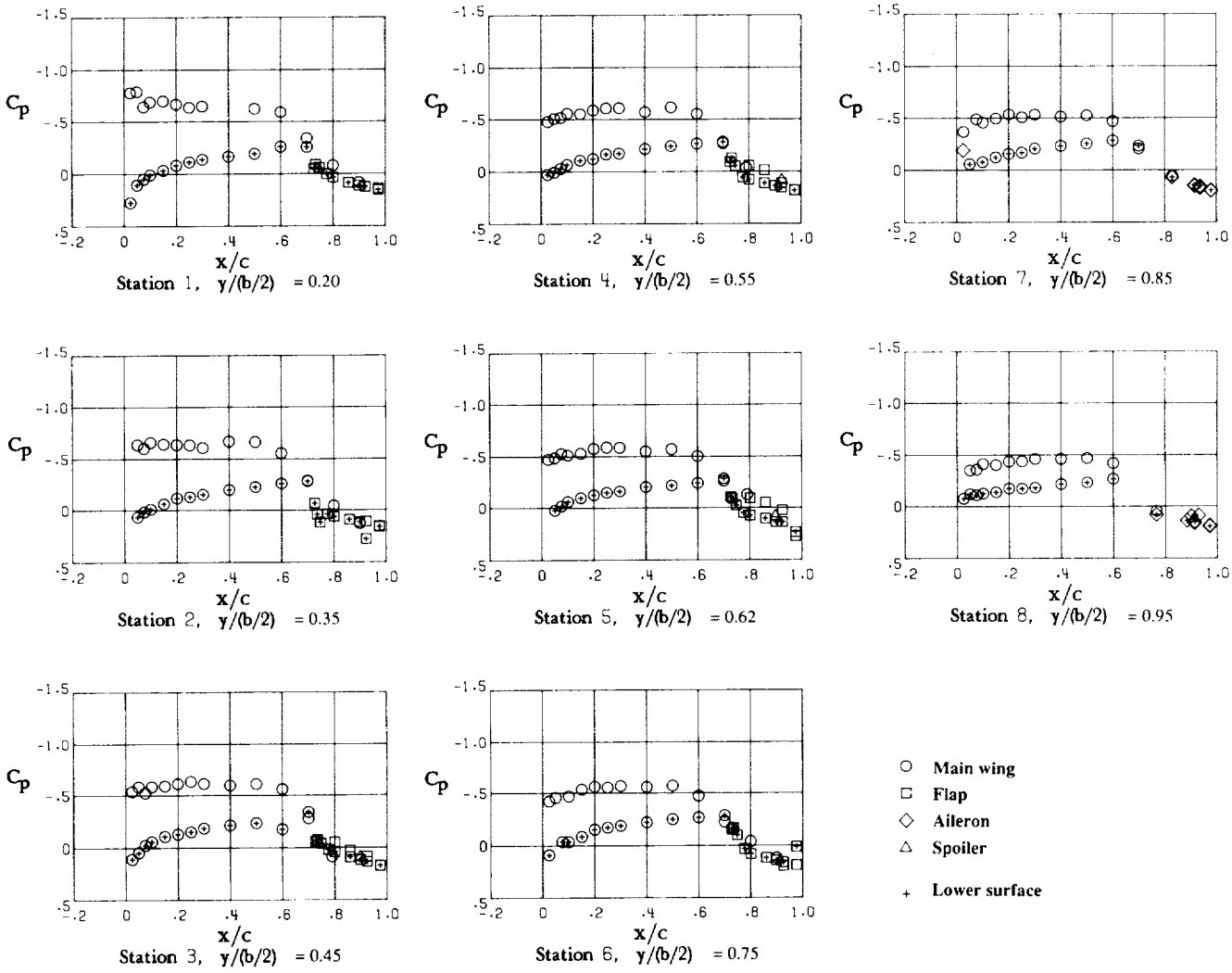

(b) $\alpha = 1.5°$.

Figure 8. Continued.

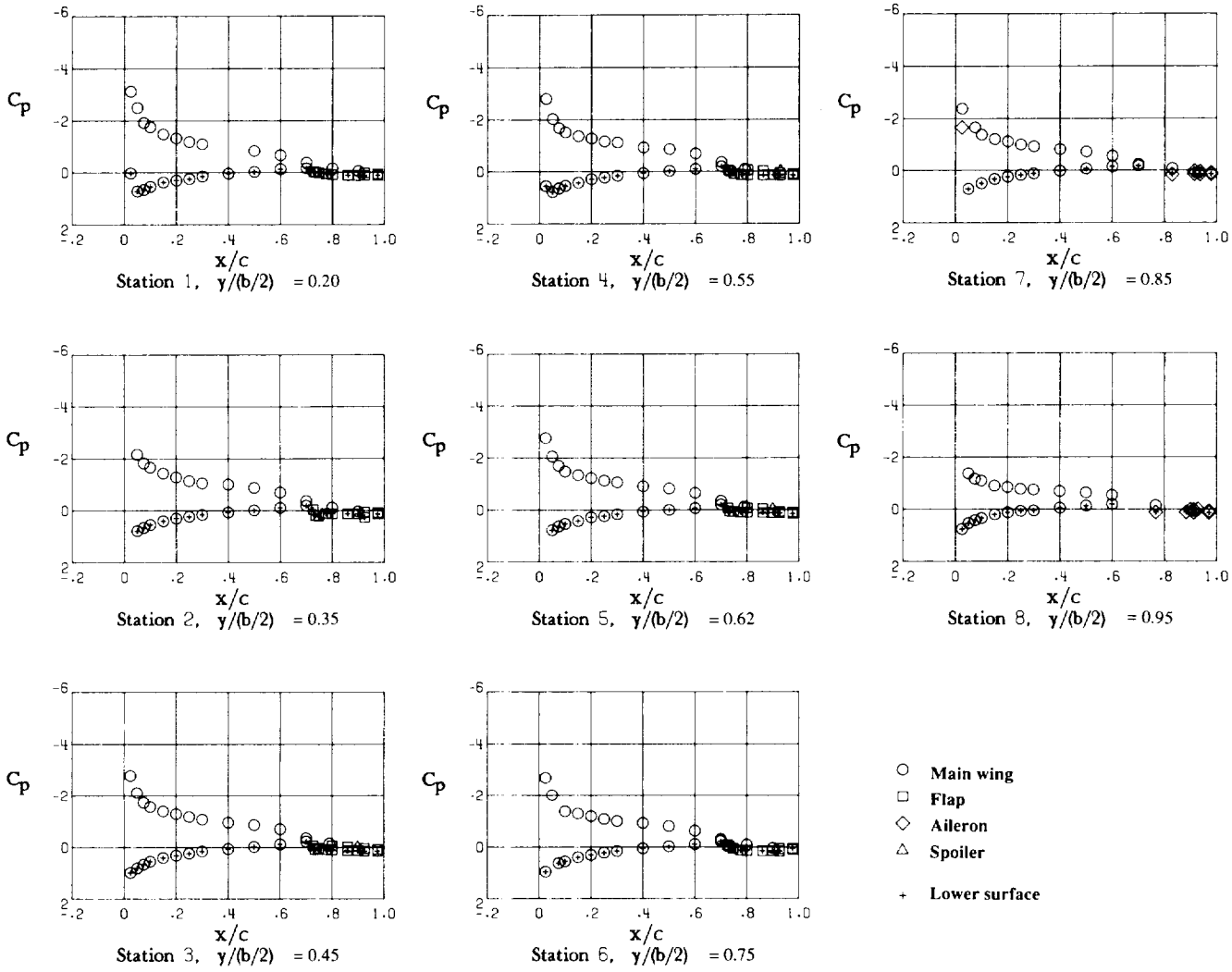

(c) $\alpha = 9.0°$.

Figure 8. Continued.

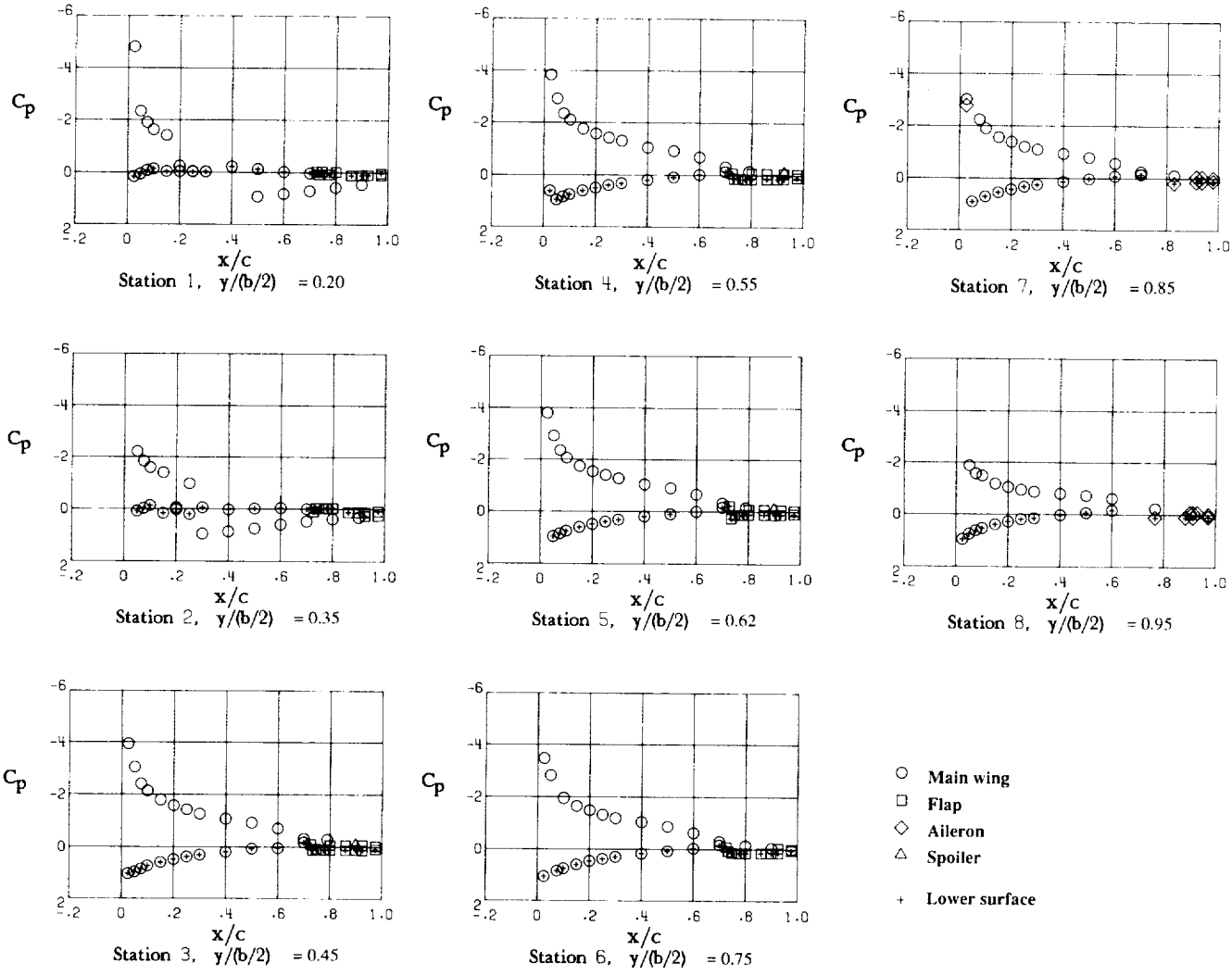

(d) $\alpha = 12.8°$.

Figure 8. Continued.

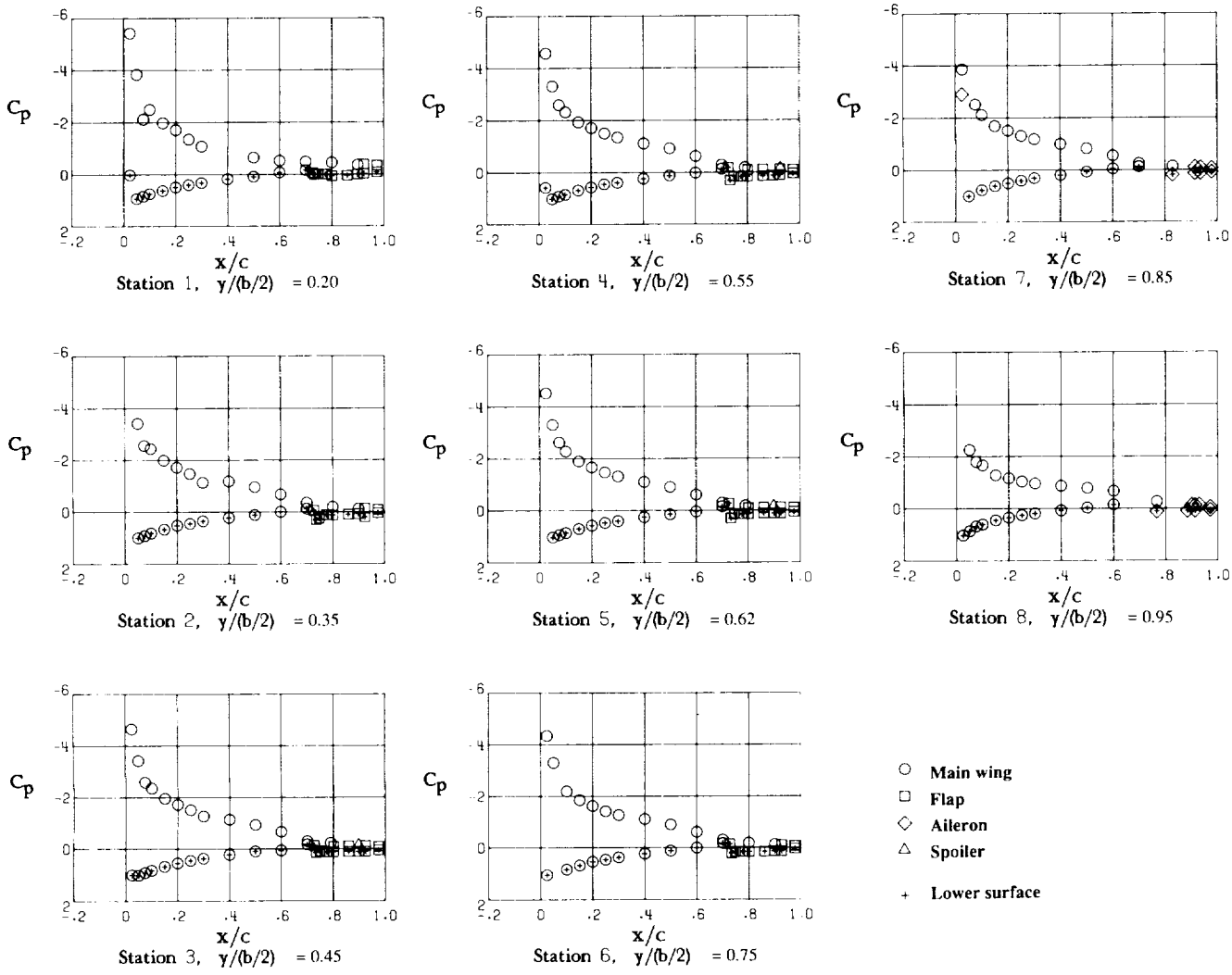

(e) $\alpha = 14.8°$.

Figure 8. Continued.

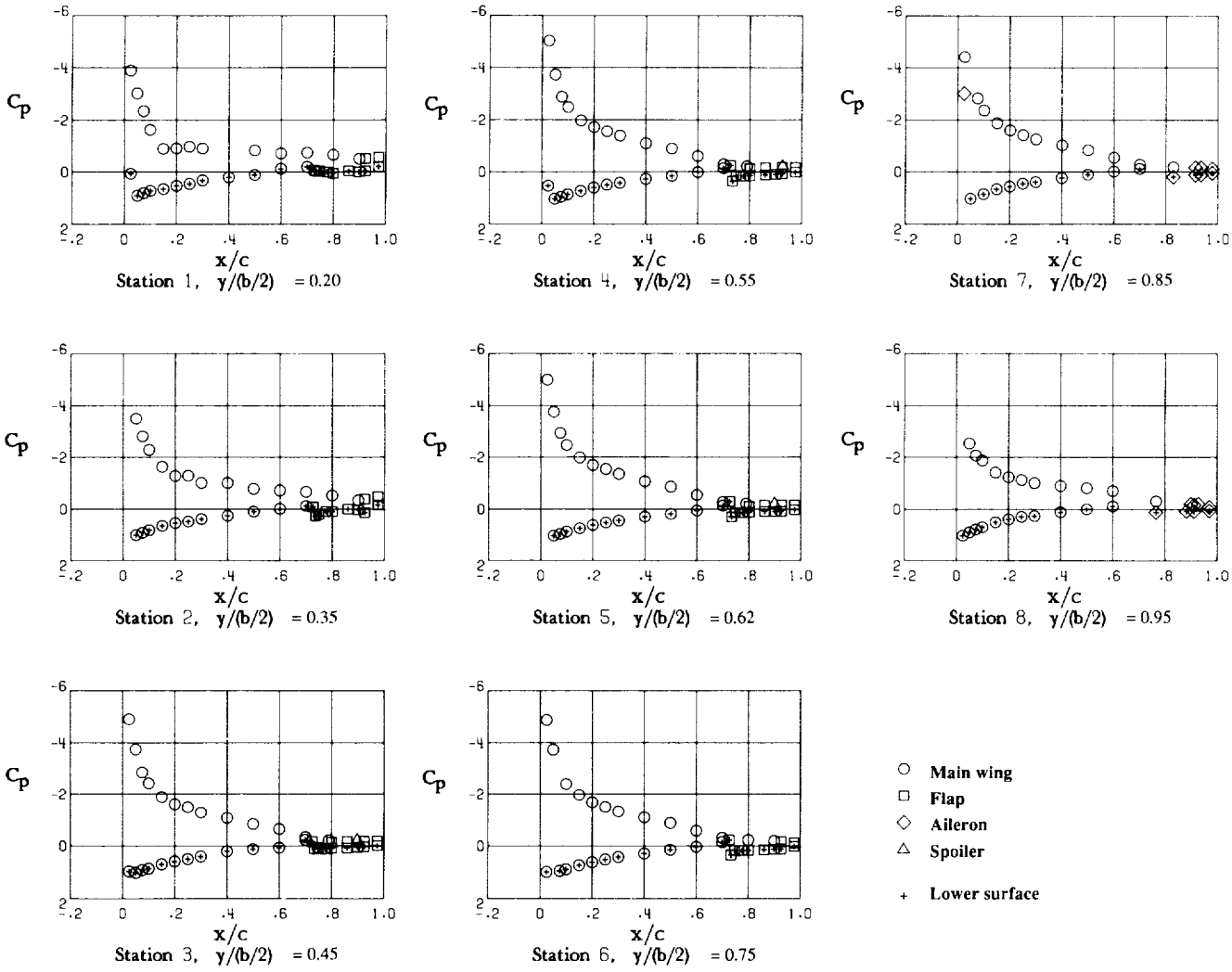

(f) $\alpha = 16.8°$.

Figure 8. Concluded.

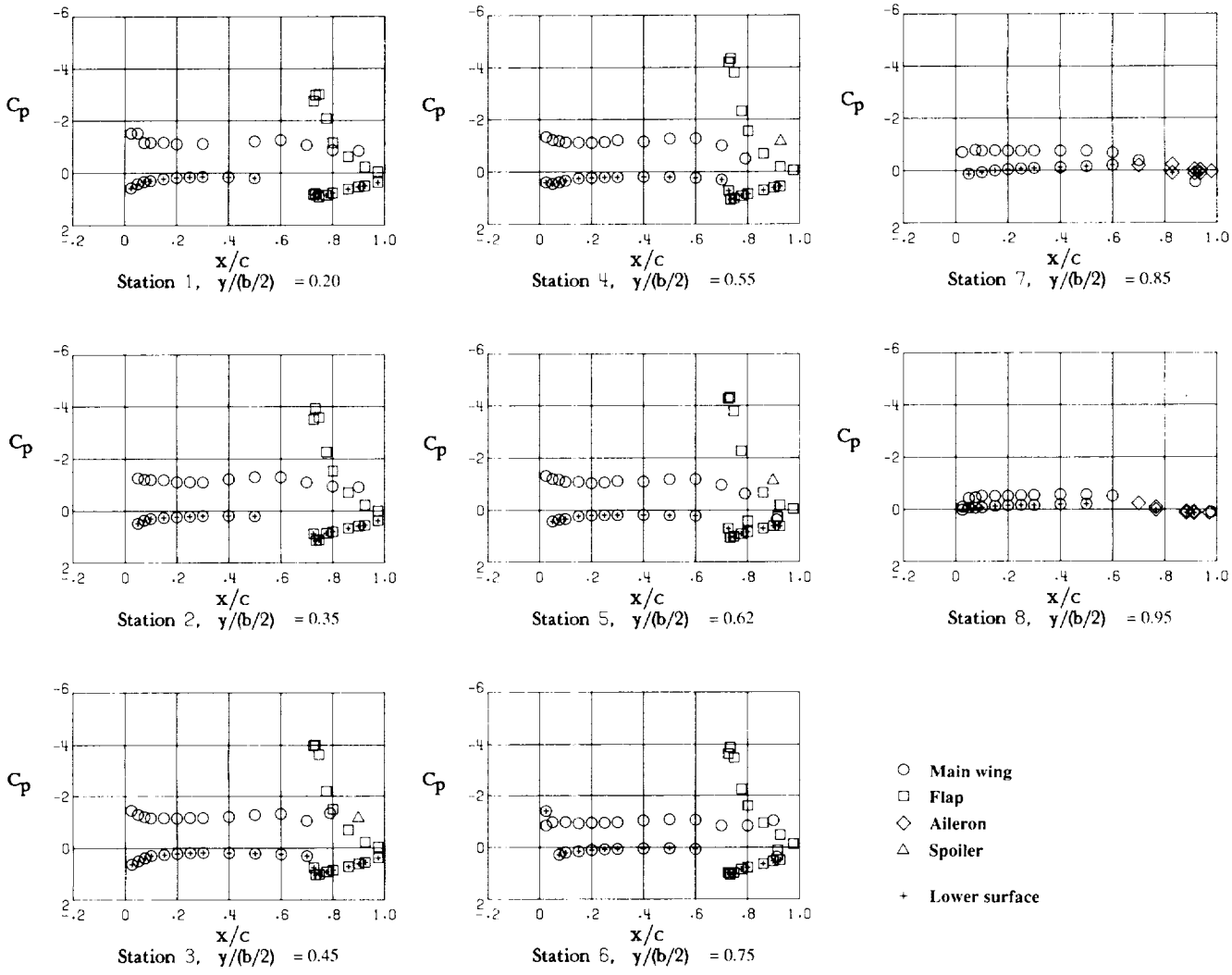

(a) $\alpha = -1.3°$.

Figure 9. Pressure distributions with flap deflected. $\delta_f = 40°$; VG on.

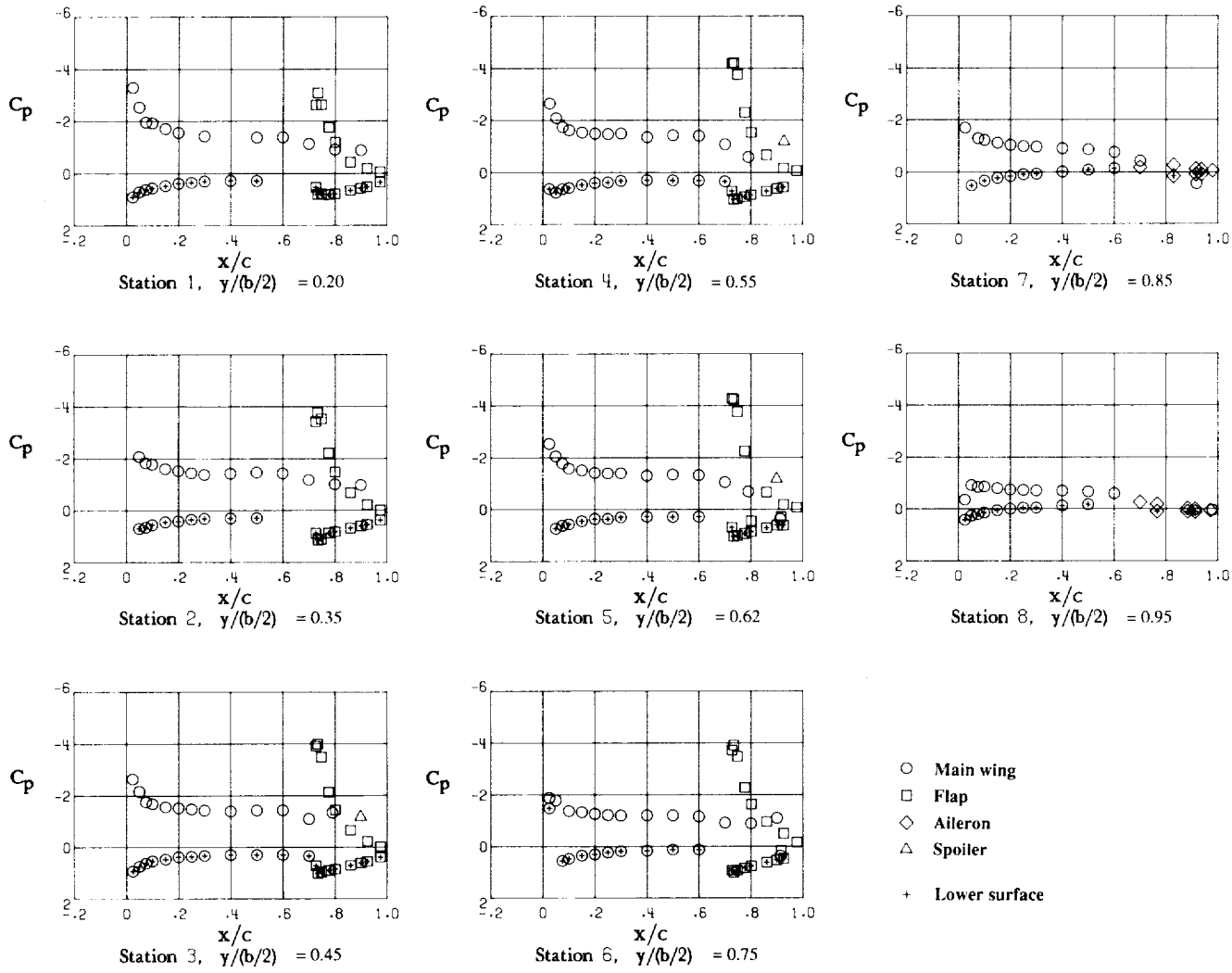

(b) $\alpha = 2.4°$.

Figure 9. Continued.

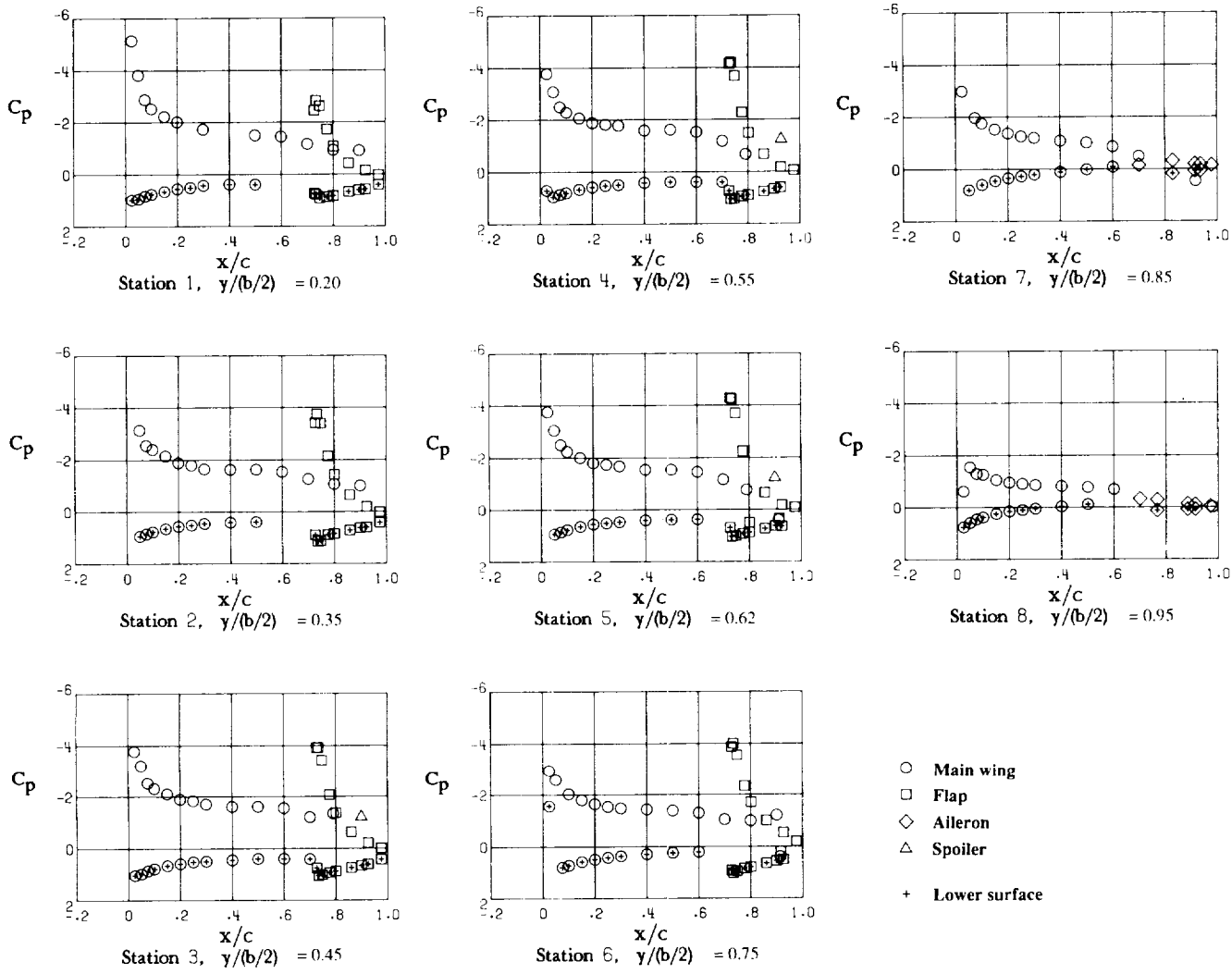

(c) $\alpha = 6.1°$.

Figure 9. Continued.

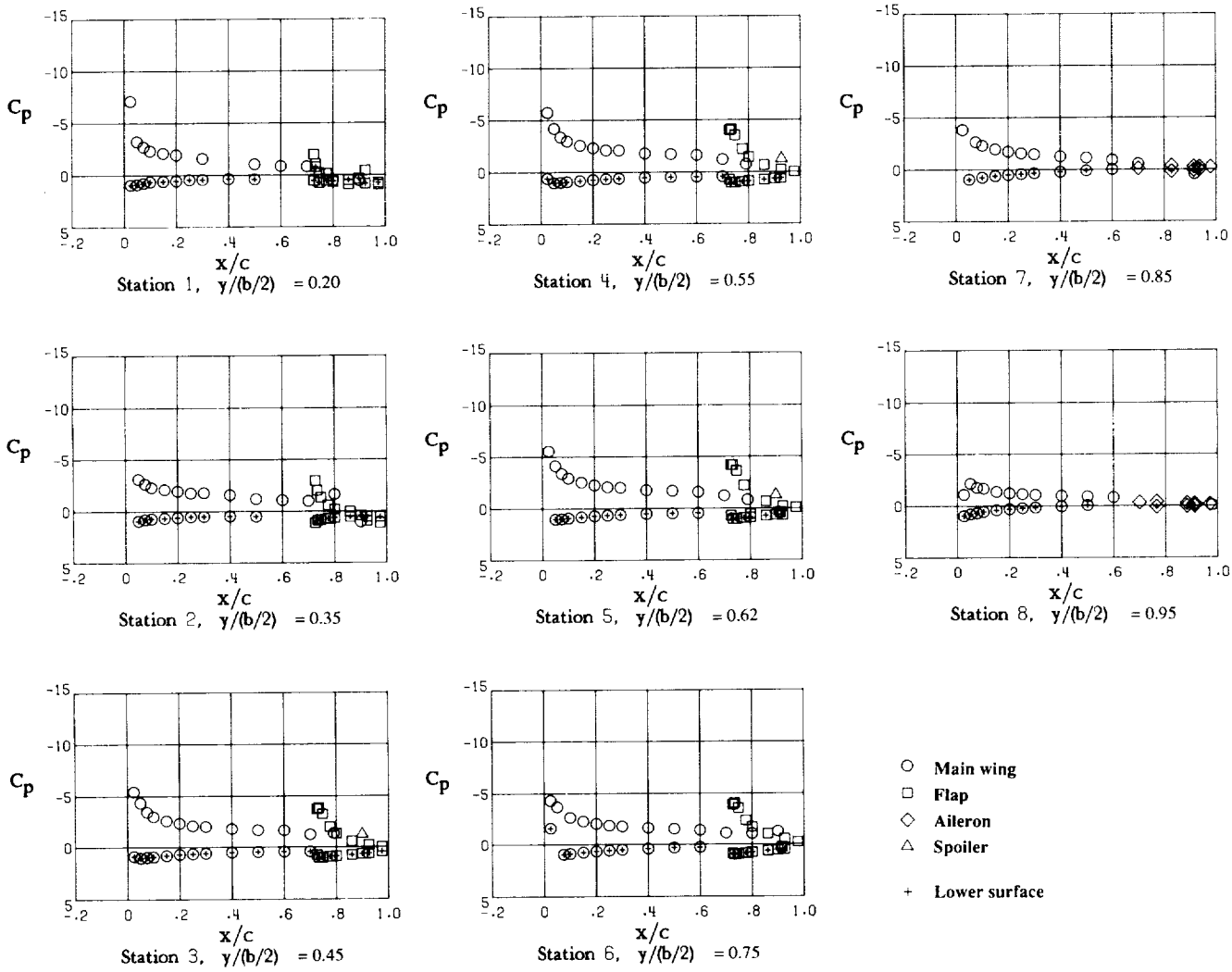

(d) $\alpha = 10.0°$.

Figure 9. Continued.

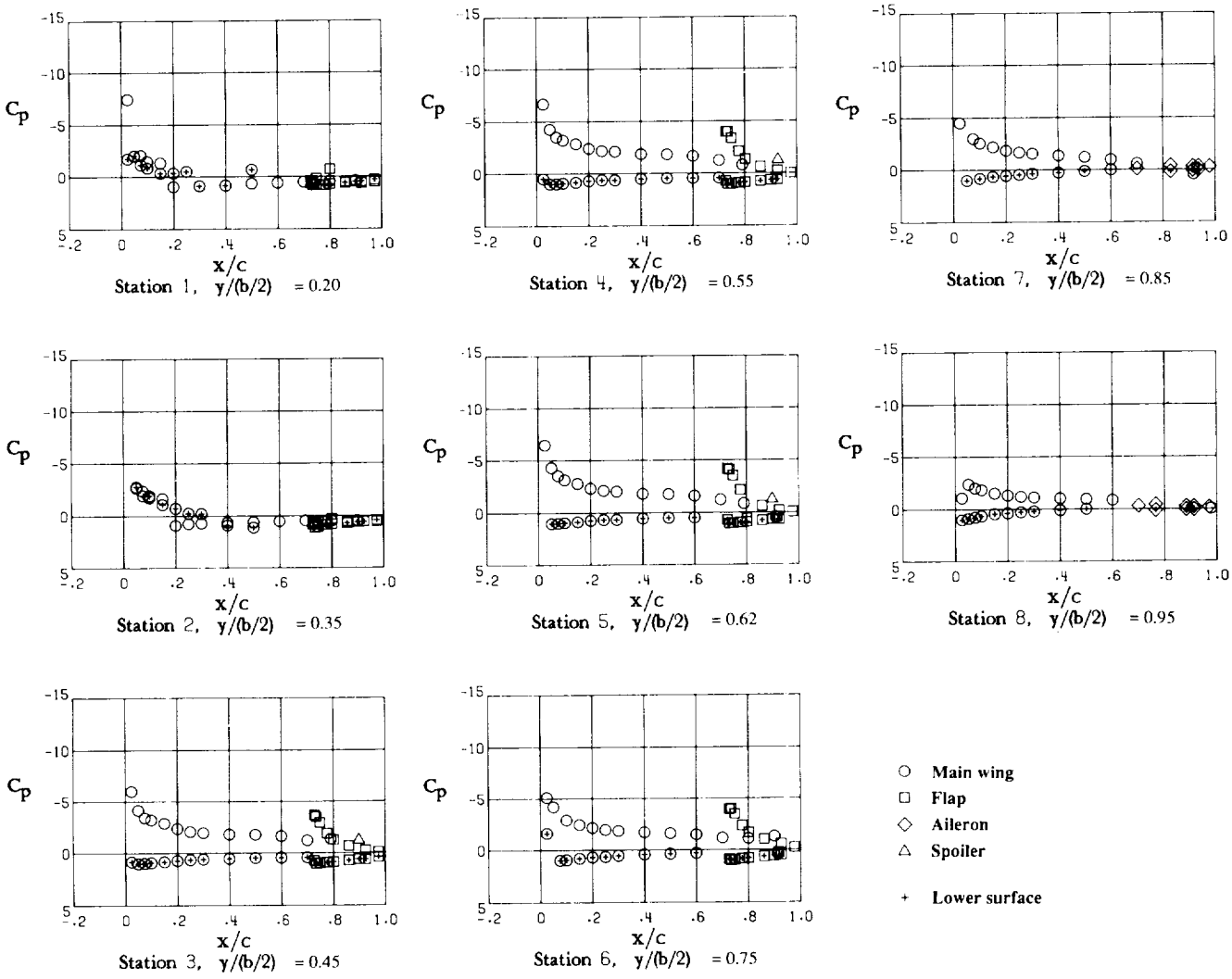

(e) $\alpha = 12.0°$.

Figure 9. Continued.

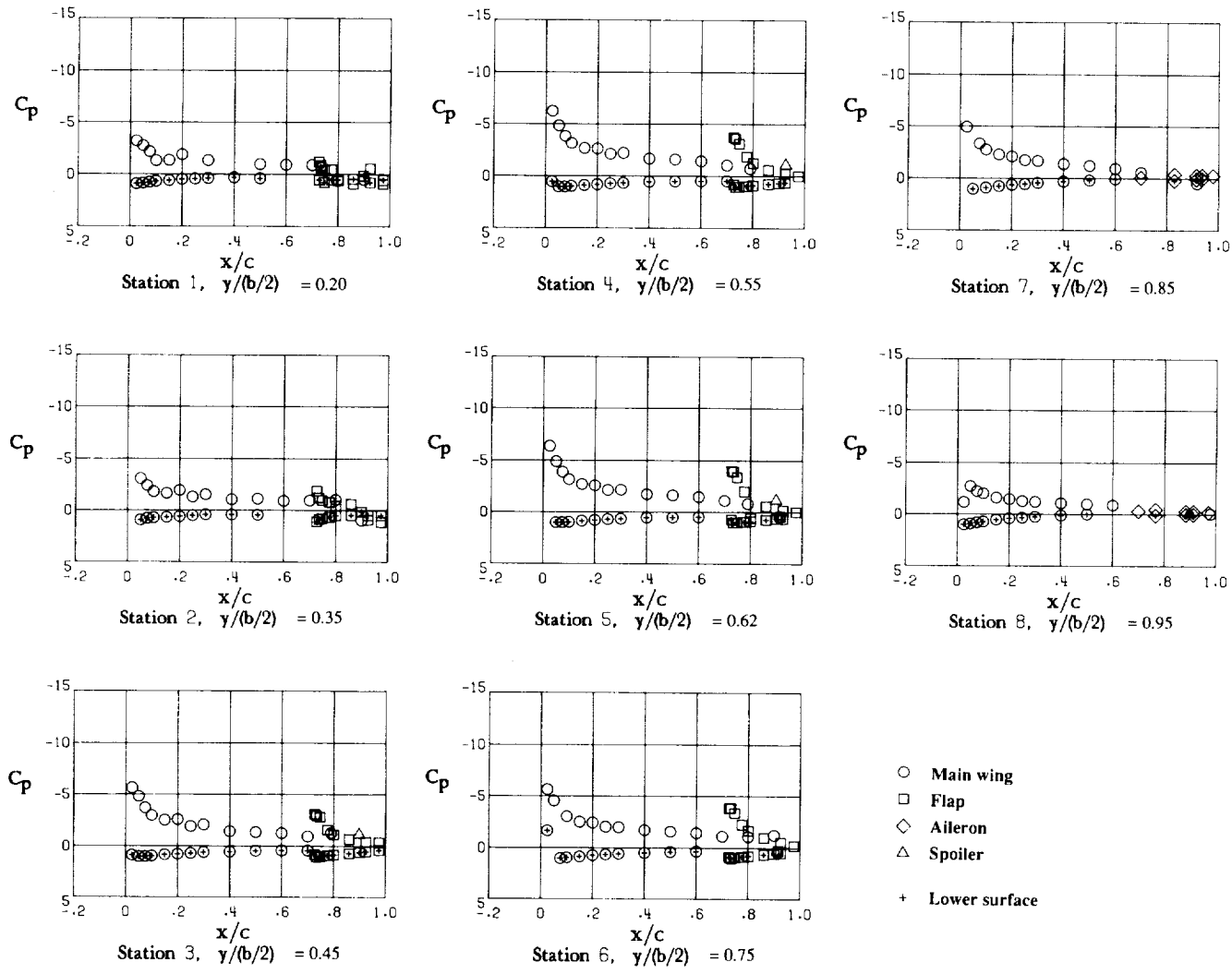

(f) $\alpha = 14.2°$.

Figure 9. Continued.

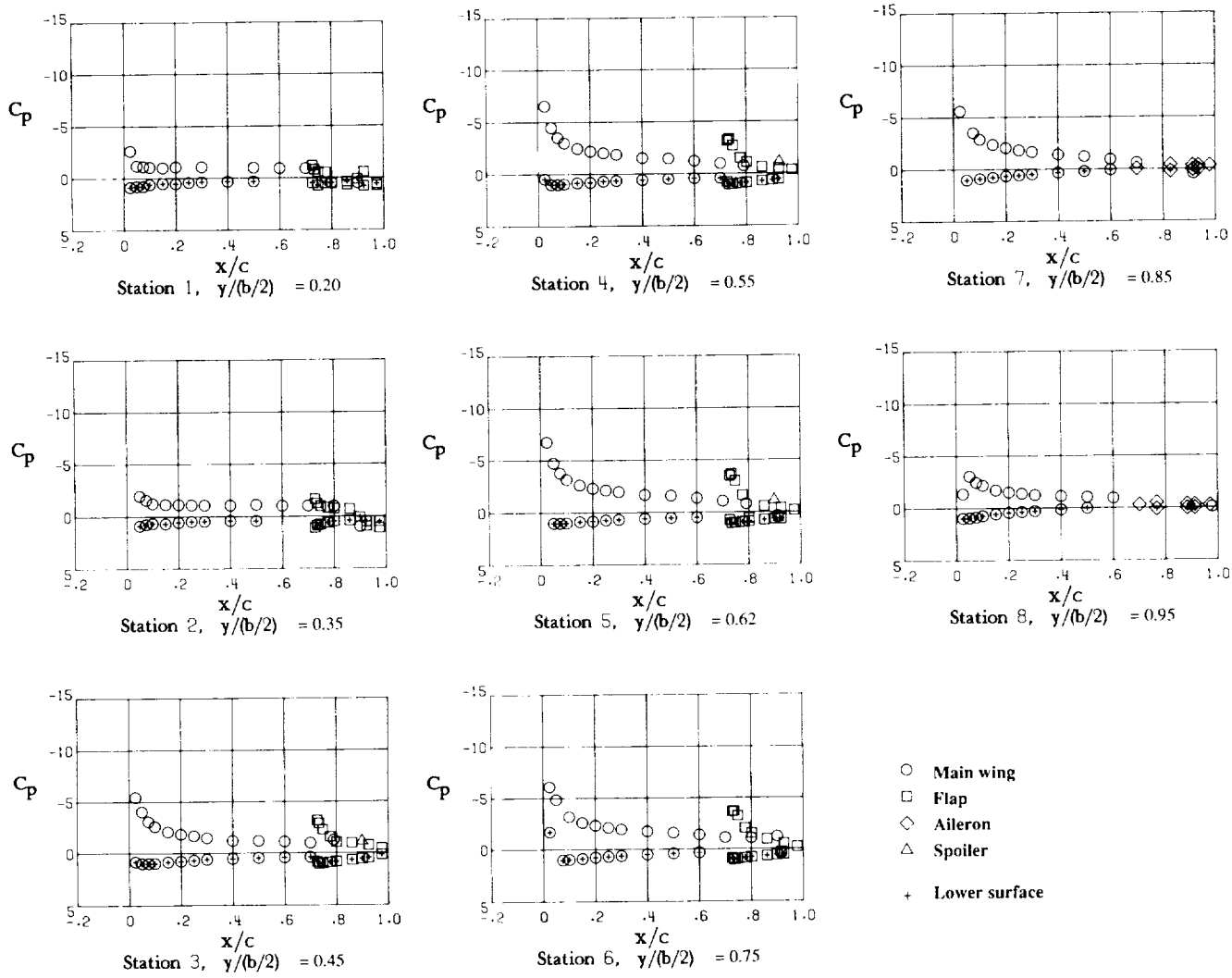

(g) $\alpha = 16.2°$.

Figure 9. Concluded.

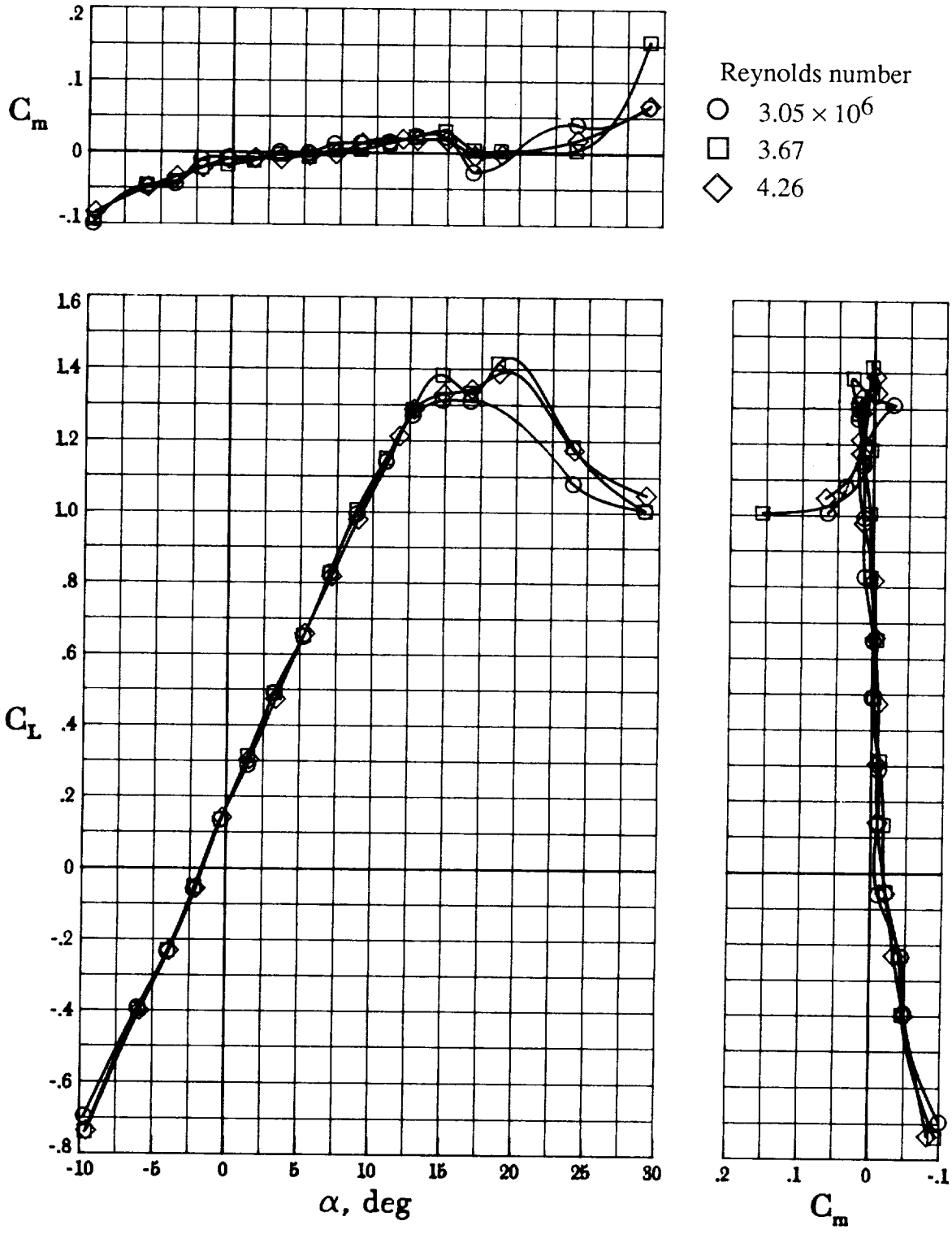

(a) Lift and pitching moment.

Figure 10. Effect of Reynolds number with flap undeflected. $\delta_f = 0°$; VG off.

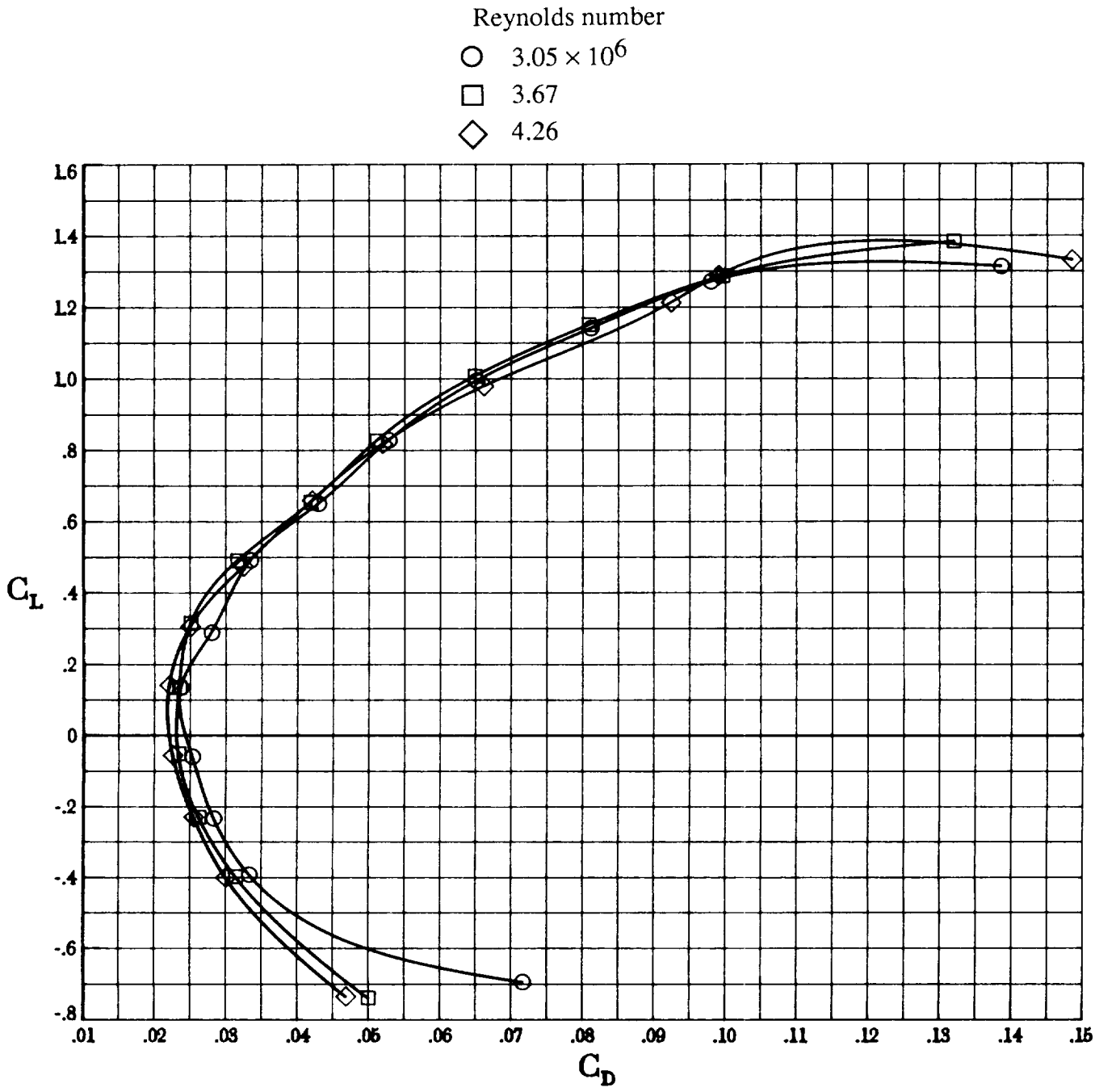

(b) Drag polar.

Figure 10. Concluded.

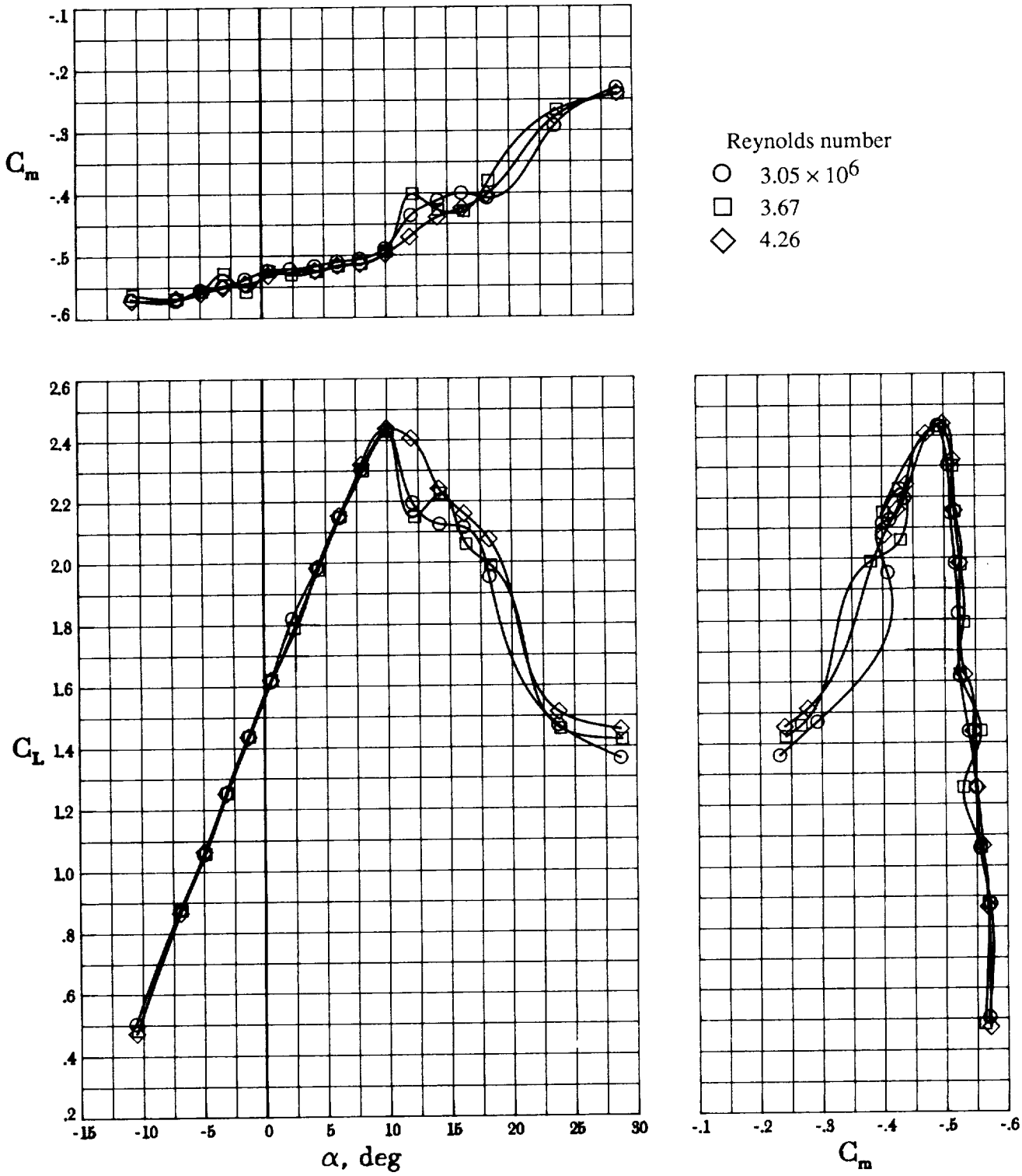

Figure 11. Effect of Reynolds number with flap deflected. $\delta_f = 40°$; VG on.

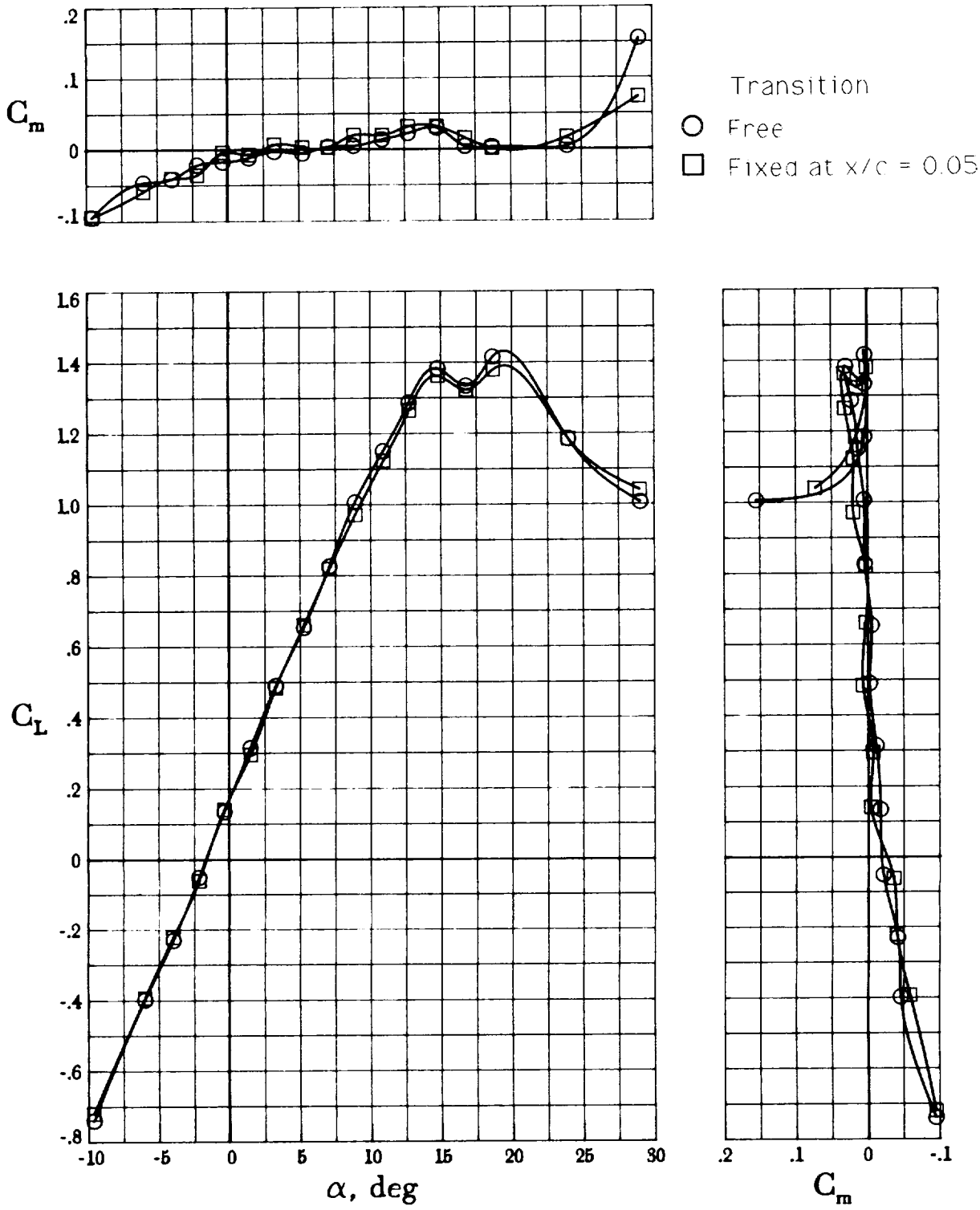

(a) Lift and pitching moment.

Figure 12. Effect of fixed transition with flap undeflected. $\delta_f = 0°$; VG off.

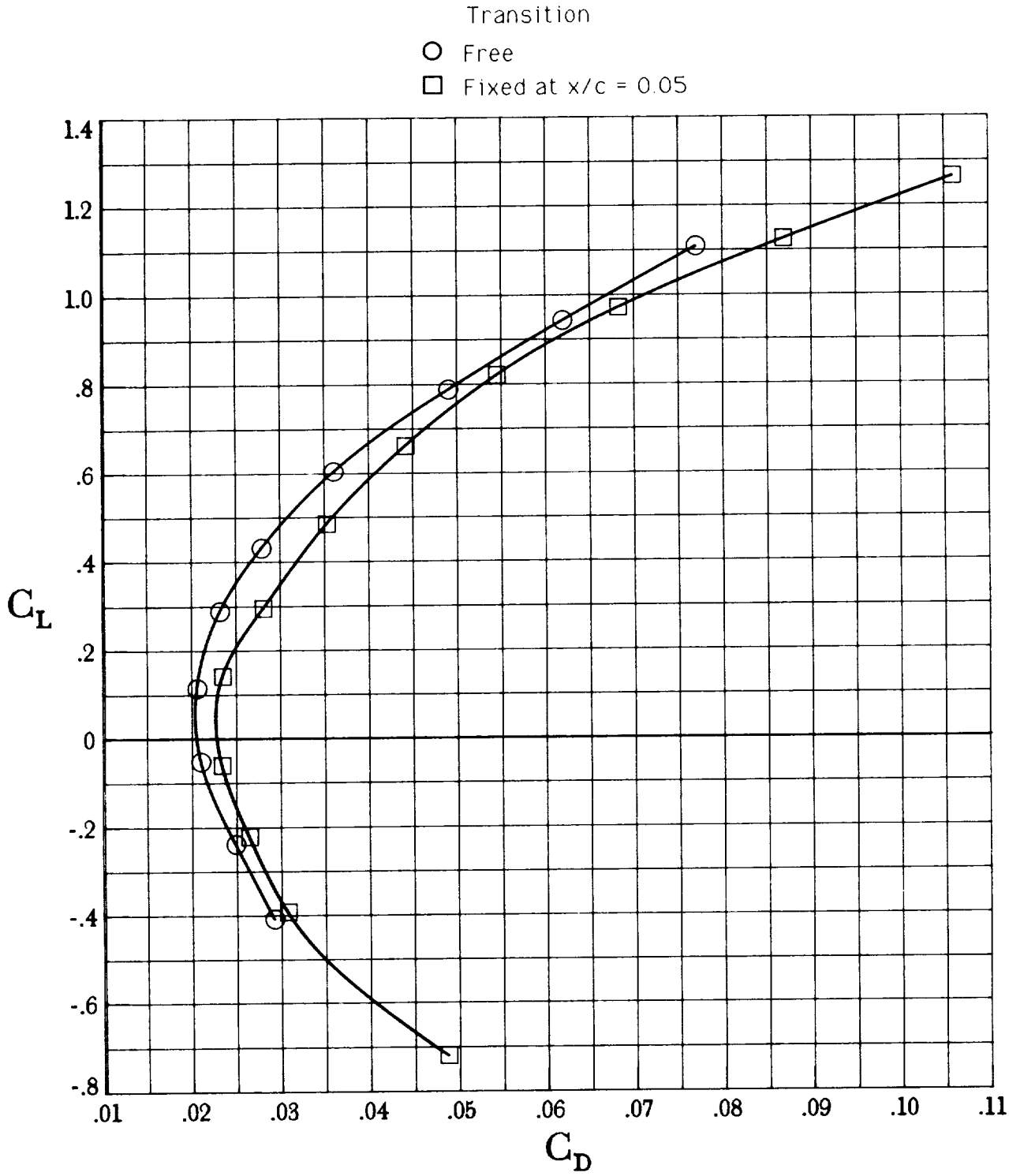

(b) Drag polar.

Figure 12. Concluded.

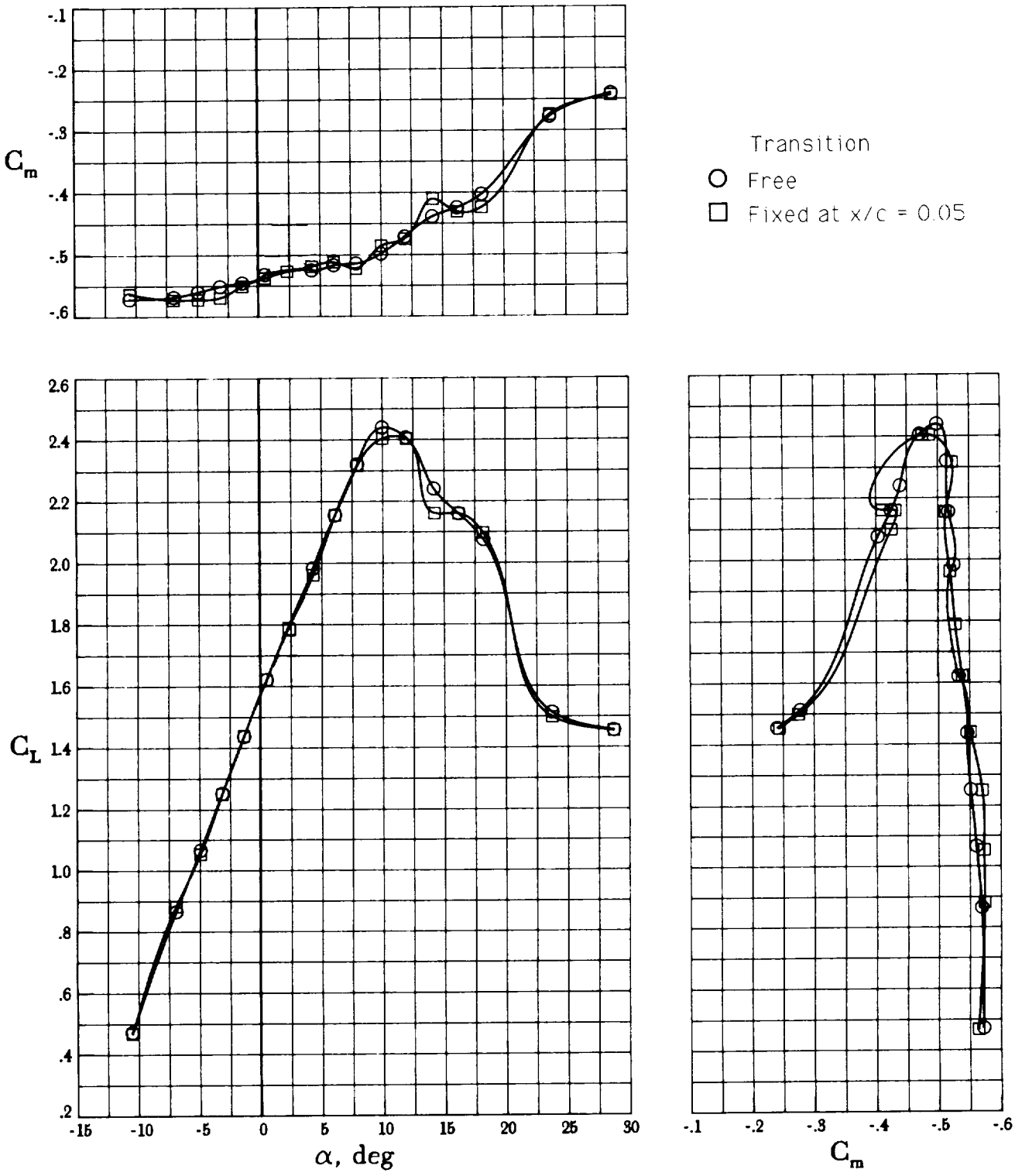

Figure 13. Effect of transition with flap deflected. $\delta_f = 40°$; VG on.

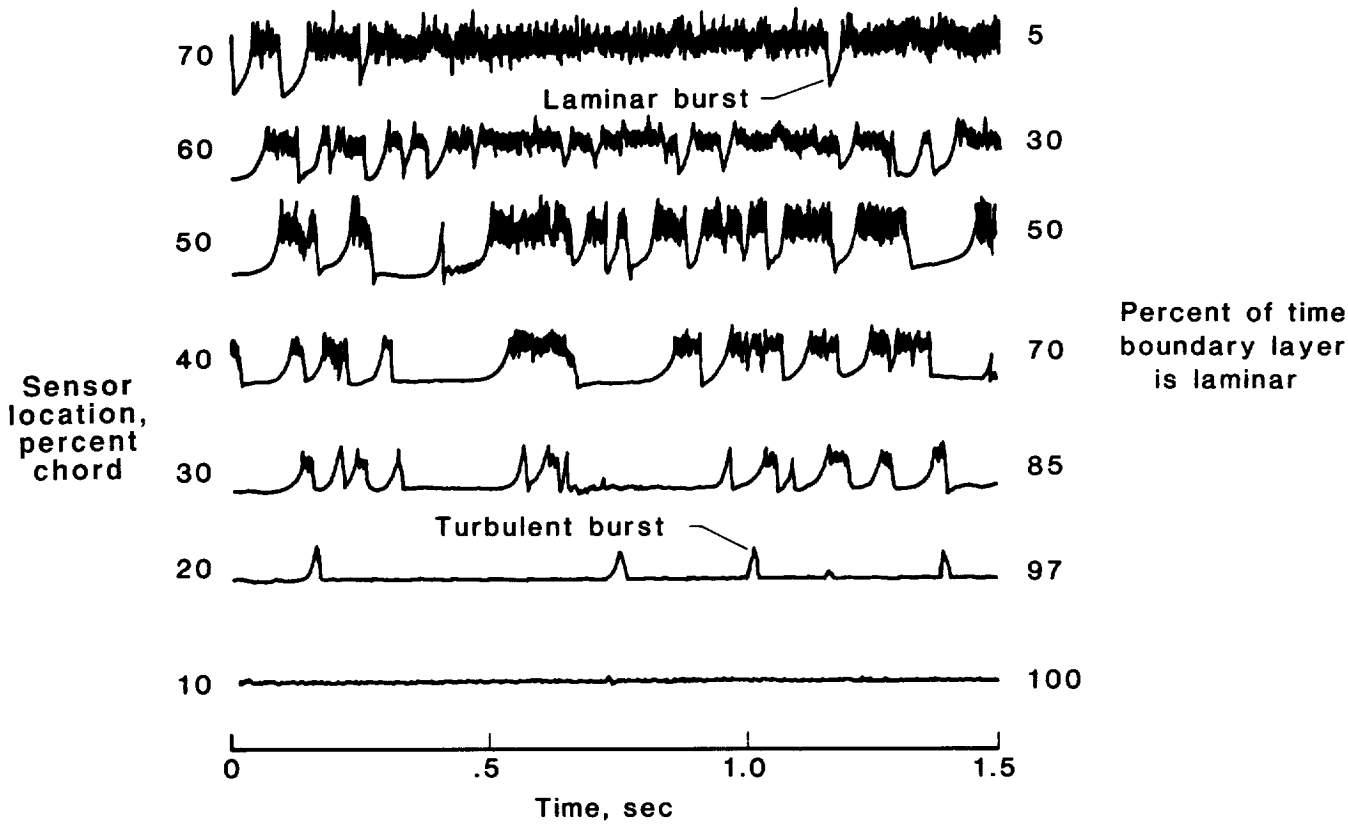

Figure 14. Sample trace of hot-film data. $C_L = 0.22; \delta_f = 0°$; VG off.

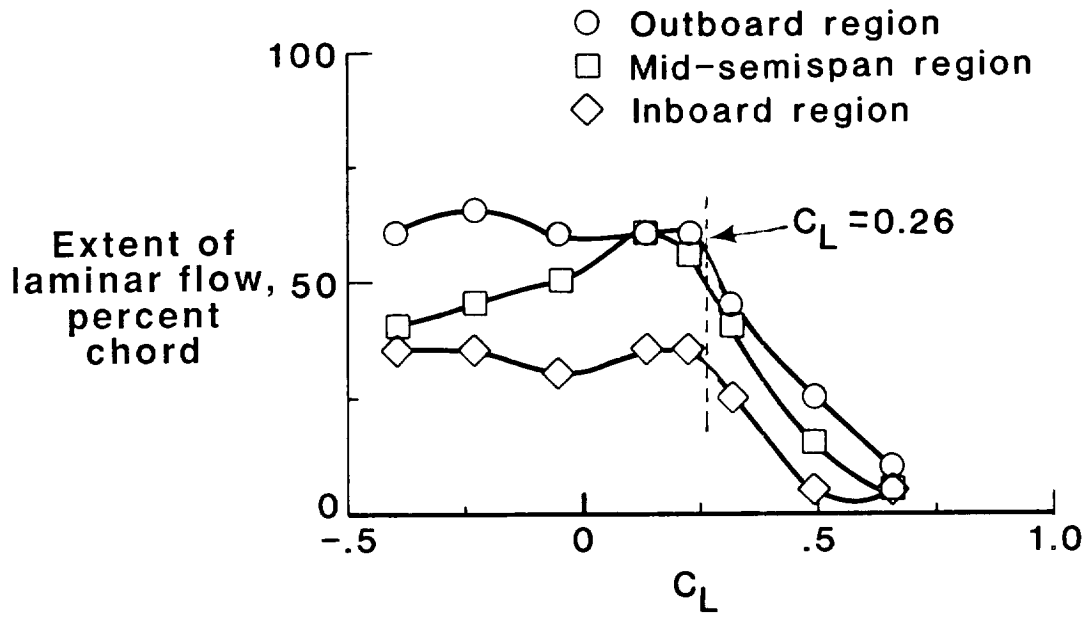

(a) Upper surface.

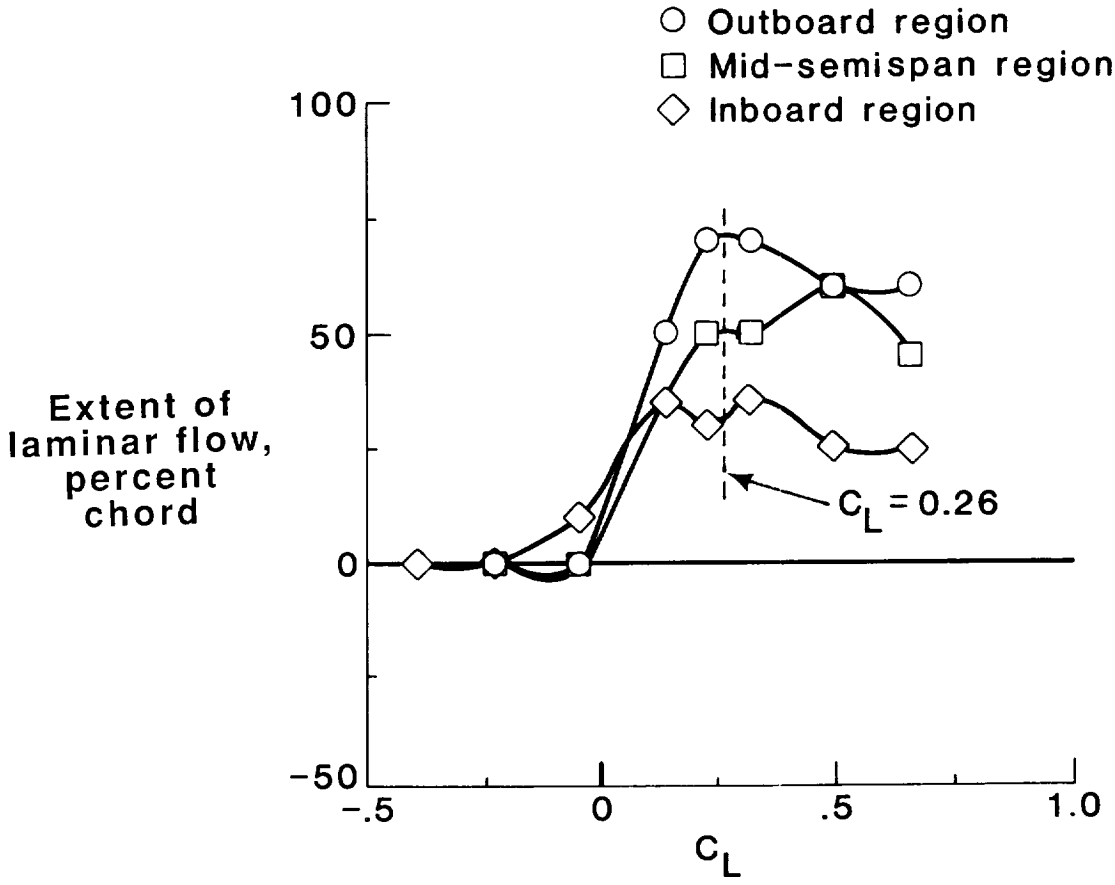

(b) Lower surface.

Figure 15. Extent of laminar flow on wing with flap undeflected. $\delta_f = 0°$; VG off.

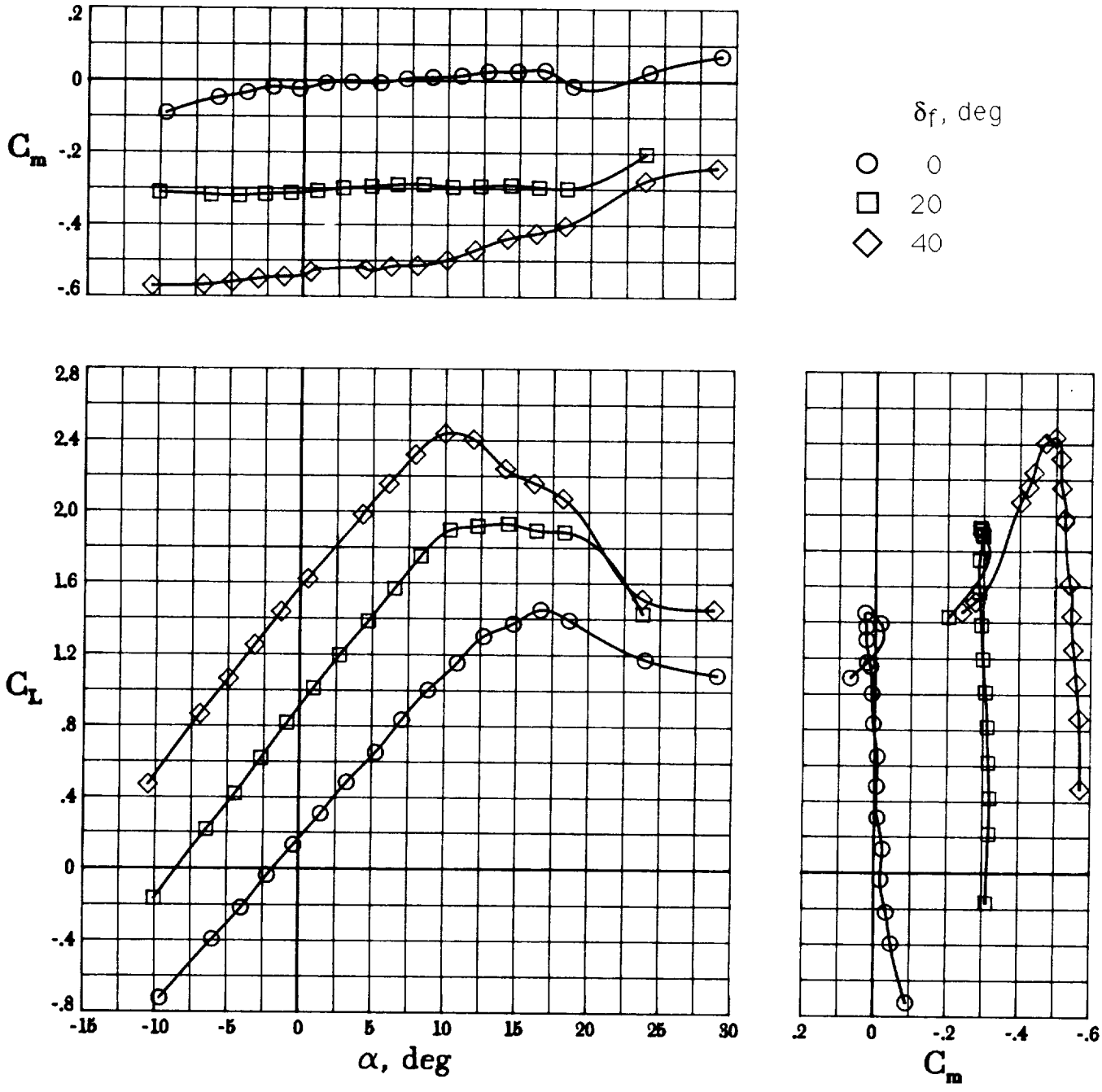

(a) Lift and pitching moment.

Figure 16. Effect of flap deflection. VG on.

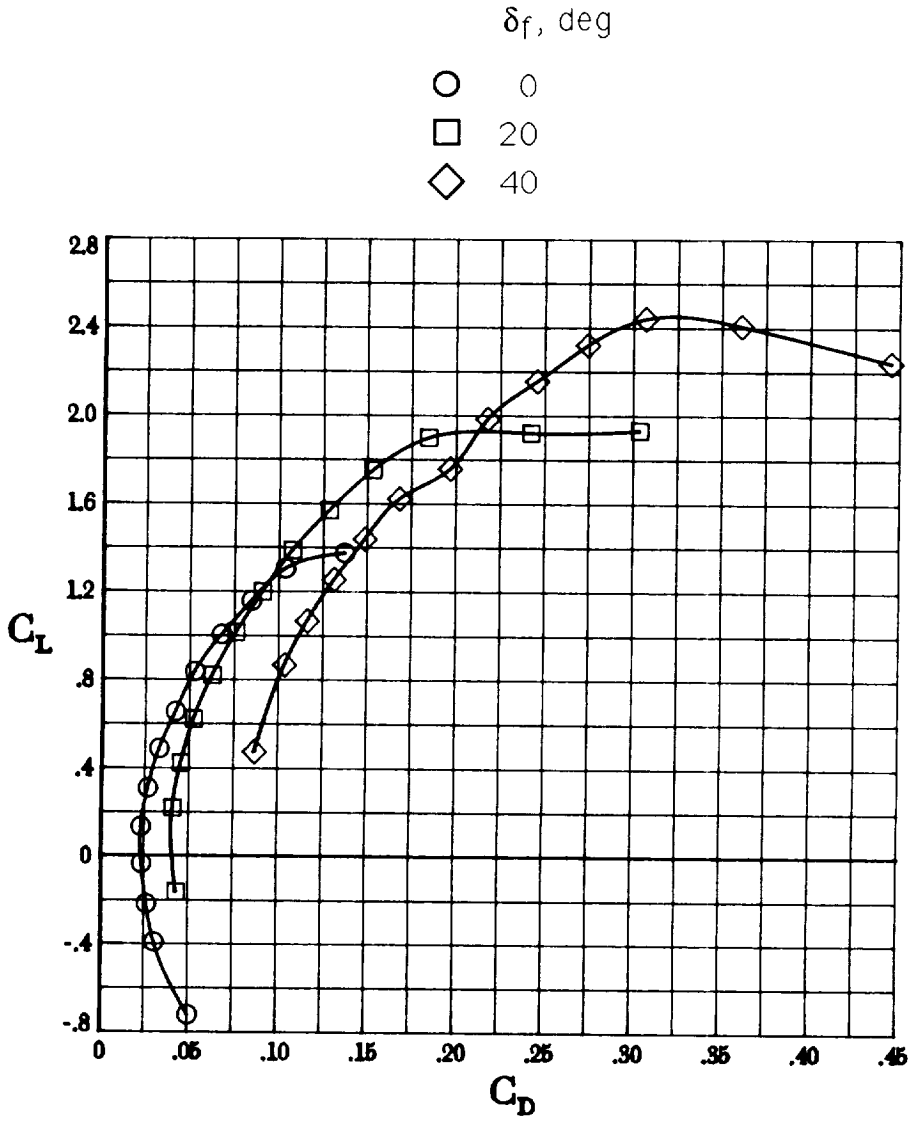

(b) Drag polar.

Figure 16. Concluded.

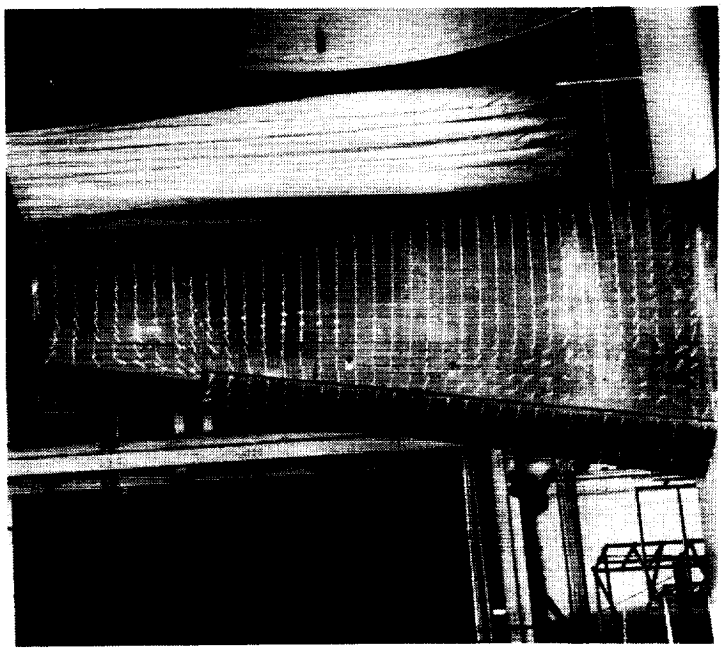

(b) VG on.

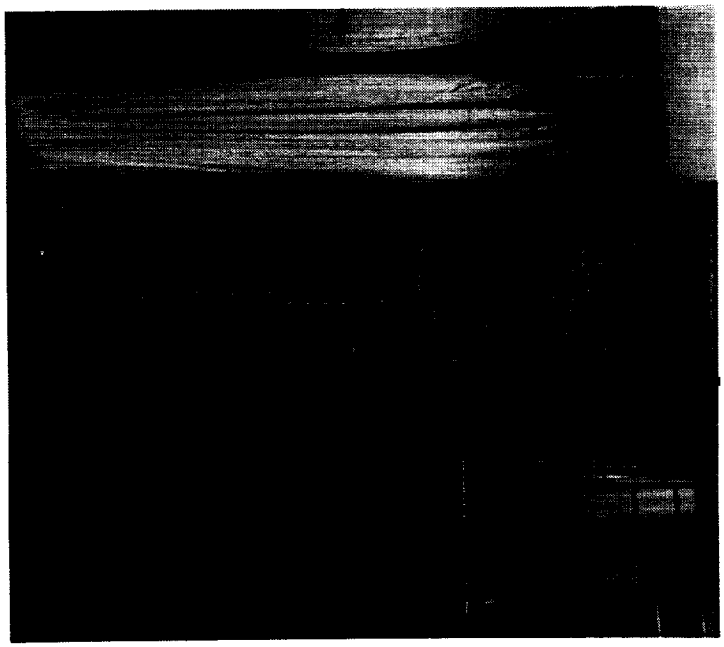

(a) VG off.

L-91-60

Figure 17. Flow visualization of effect of vortex generator. $\delta_f = 40°; \alpha = 11.9°$.

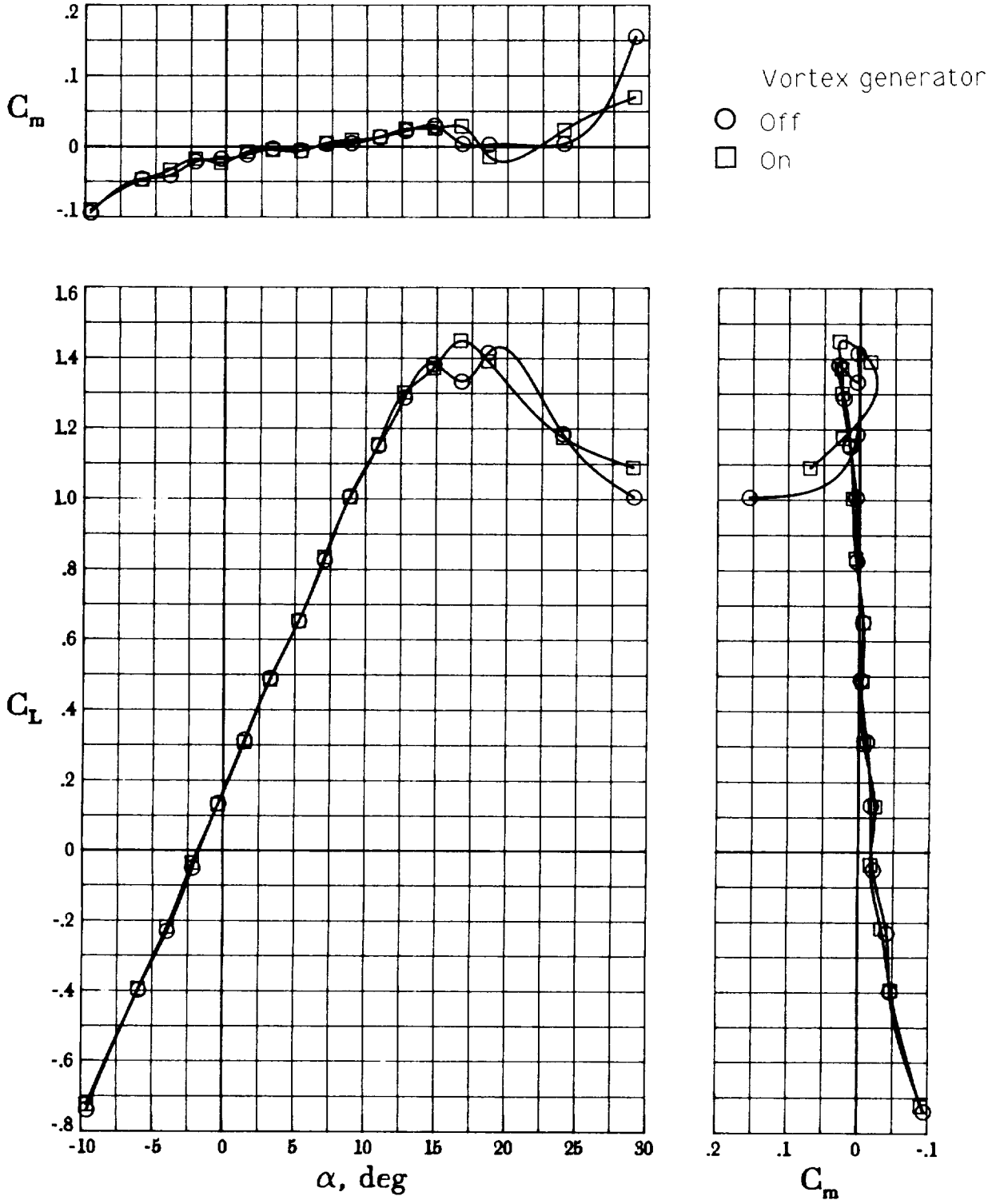

(a) Lift and pitching moment.

Figure 18. Effect of vortex generator with flap undeflected. $\delta_f = 0°$.

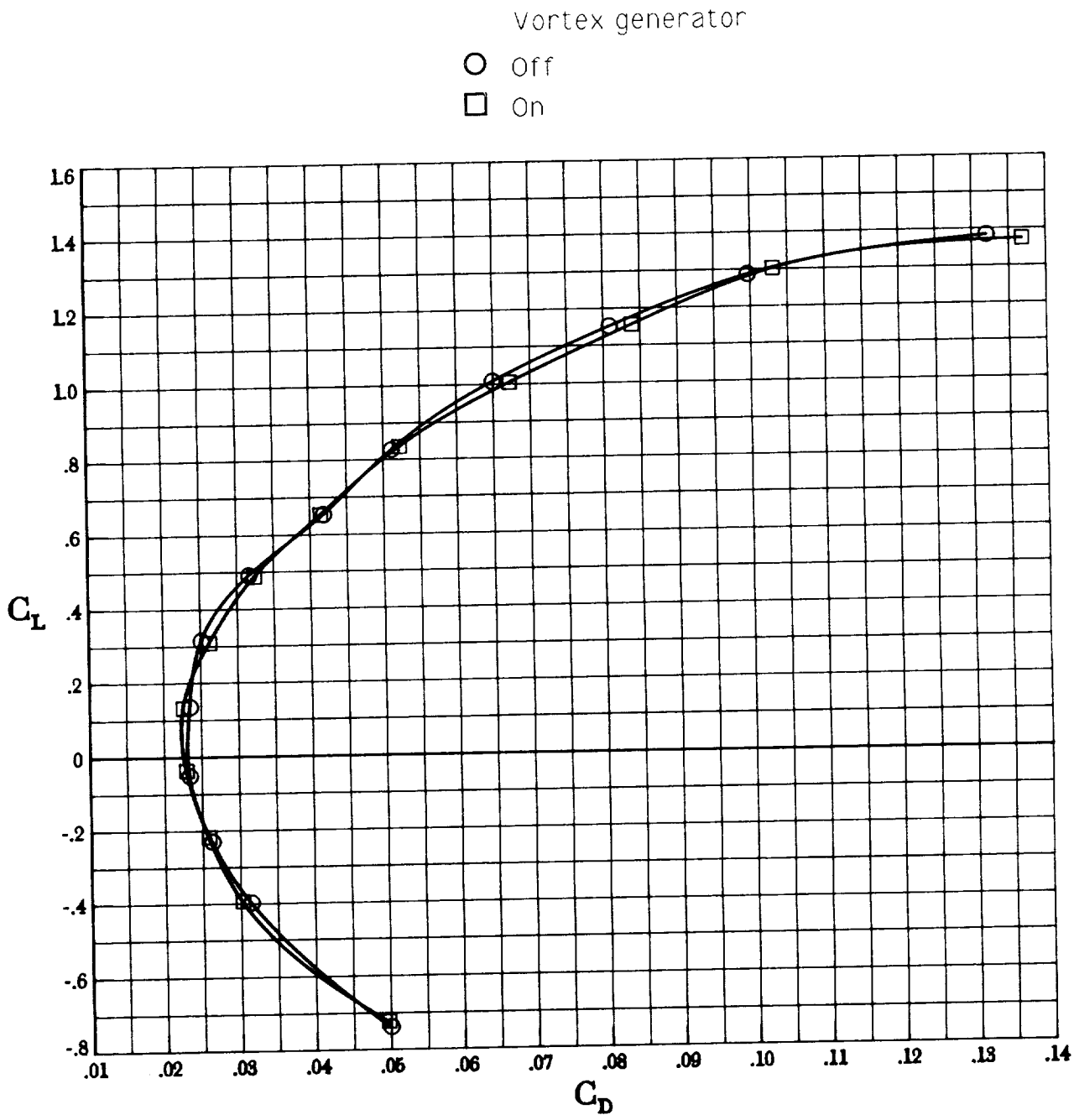

(b) Drag polar.

Figure 18. Concluded.

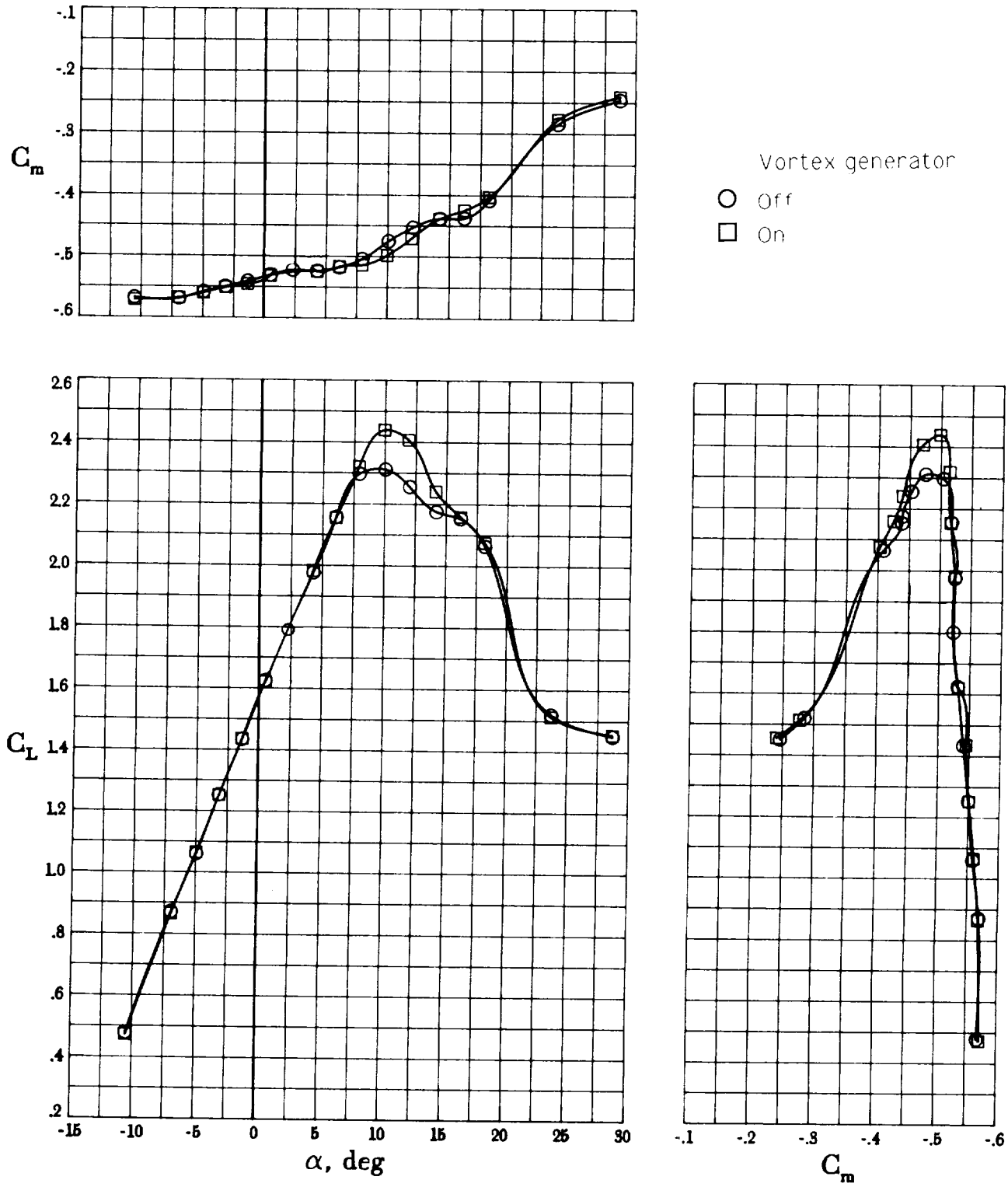

Figure 19. Effect of vortex generator with flap deflected. $\delta_f = 40°$.

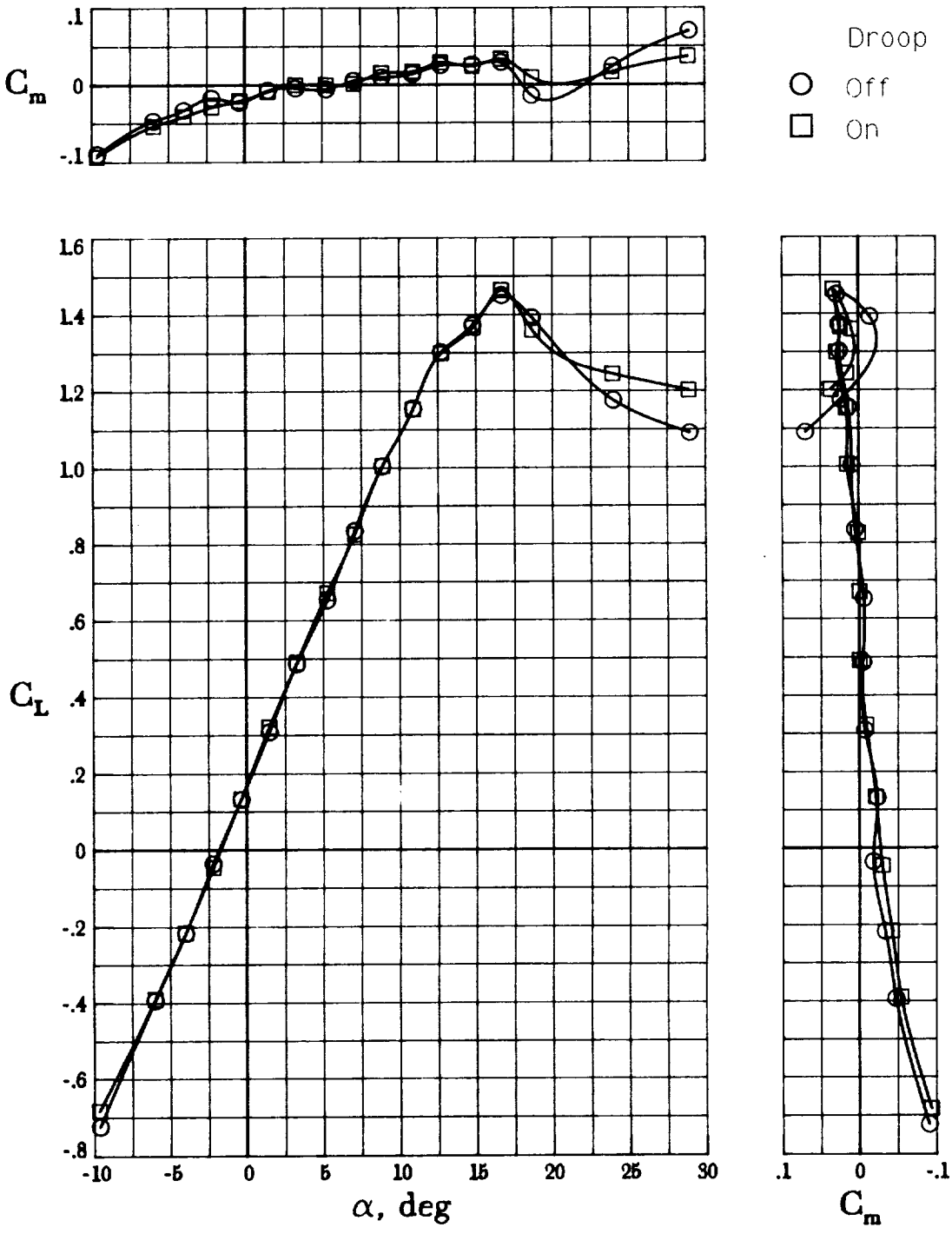

(a) Lift and pitching moment.

Figure 20. Effect of leading-edge droop with flap undeflected. $\delta_f = 0°$; VG on.

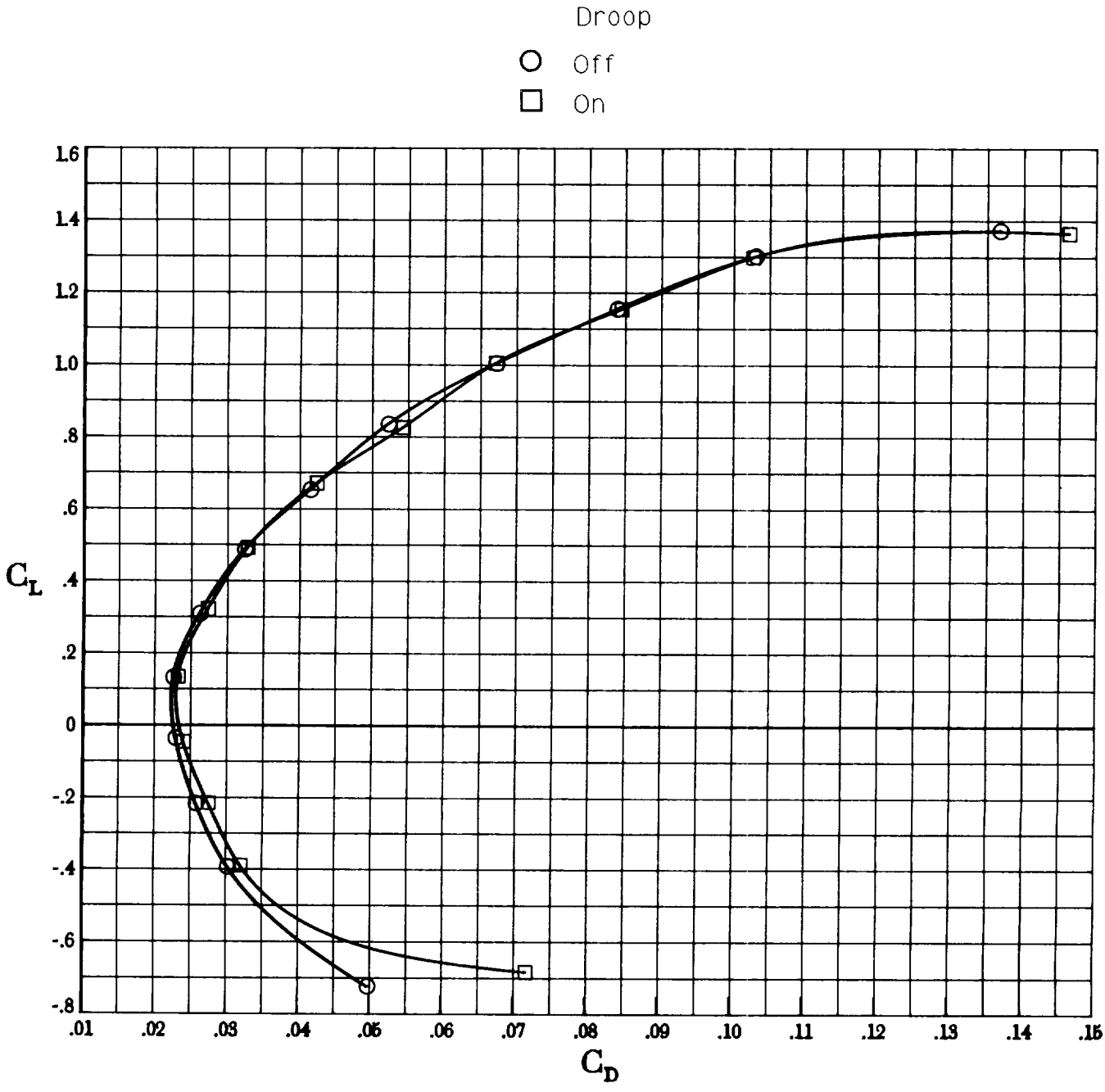

(b) Drag polar.

Figure 20. Concluded.

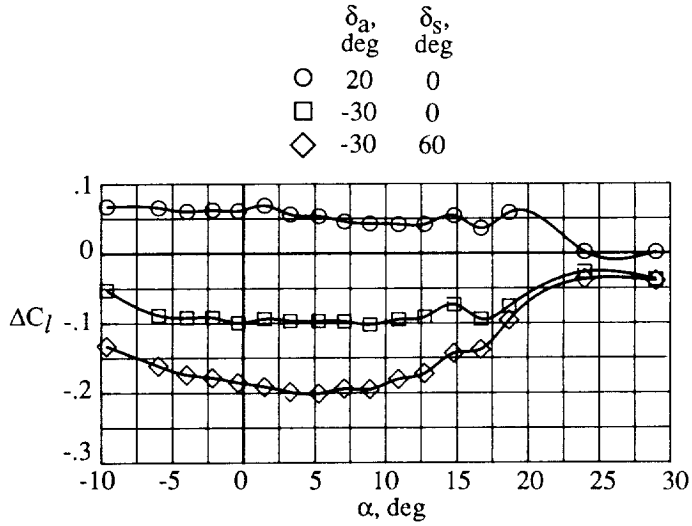

Figure 21. Roll-control effectiveness with flap undeflected. $\delta_f = 0°$; VG on.

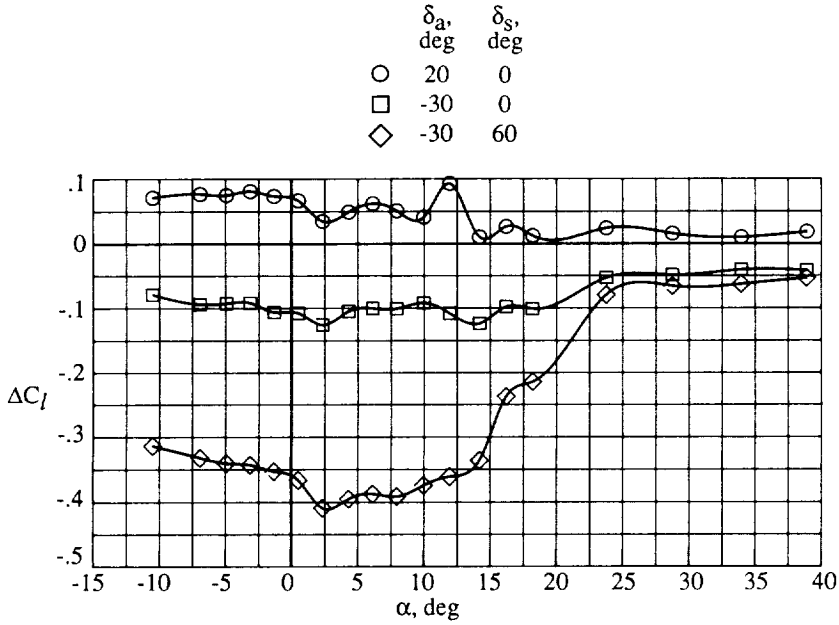

Figure 22. Roll-control effectiveness with flap undeflected. $\delta_f = 40°$; VG on.

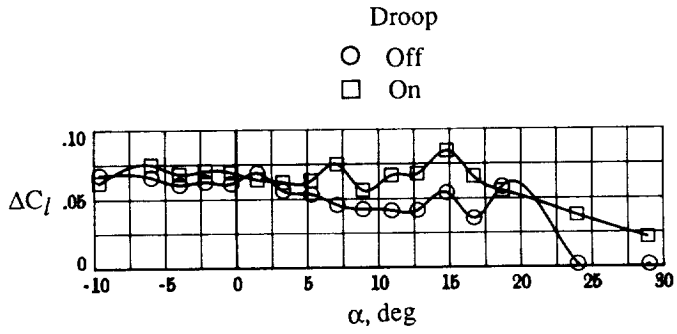

Figure 23. Effect of leading-edge droop on roll control with flap undeflected. $\delta_f = 0°$; $\delta_a = 20°$; VG on.

NASA
National Aeronautics and Space Administration

Report Documentation Page

1. Report No.	2. Government Accession No.	3. Recipient's Catalog No.
NASA TP-3133		

4. Title and Subtitle	5. Report Date
Full-Scale Semispan Tests of a Business-Jet Wing With a Natural Laminar Flow Airfoil	September 1991
	6. Performing Organization Code
7. Author(s)	8. Performing Organization Report No.
David E. Hahne and Frank L. Jordan, Jr.	L-16905
9. Performing Organization Name and Address	10. Work Unit No.
NASA Langley Research Center Hampton, VA 23665-5225	505-61-41-01
	11. Contract or Grant No.
12. Sponsoring Agency Name and Address	13. Type of Report and Period Covered
National Aeronautics and Space Administration Washington, DC 20546-0001	Technical Paper
	14. Sponsoring Agency Code

15. Supplementary Notes

16. Abstract

An investigation was conducted in the Langley 30- by 60-Foot Tunnel on a full-scale semispan model to evaluate and document the low-speed, high-lift characteristics of a business-jet class wing that utilized the HSNLF(1)-0213 airfoil section and a single-slotted flap system. In addition to the high-lift studies, boundary-layer transition effects were examined, a segmented leading-edge droop for improved stall/spin resistance was studied, and two roll-control devices were evaluated. The wind-tunnel investigation showed that deployment of a single-slotted, trailing-edge flap was effective in providing substantial increments in lift required for takeoff and landing performance. Fixed-transition studies to investigate premature tripping of the boundary layer indicated no adverse effects on lift and pitching-moment characteristics for either the cruise or landing configuration. The full-scale results also suggested the need to further optimize the leading-edge droop design that was developed in the subscale tests.

17. Key Words (Suggested by Author(s))	18. Distribution Statement
Natural laminar flow High lift Boundary-layer transition Stall/spin resistance	Unclassified Unlimited Subject Category 02

19. Security Classif. (of this report)	20. Security Classif. (of this page)	21. No. of Pages	22. Price
Unclassified	Unclassified	49	A03

For sale by the National Technical Information Service, Springfield, Virginia 22161-2171